Title:
A billion years of temperature variability: a key driver of Earth's long-term habitability

Authors:
Kristin D. Bergmann[1*], Nicholas Boekelheide[1], Julia W. Clarke[1], Marjorie D. Cantine[1,2], Julia Wilcots[1], Noah T. Anderson[1], Adam B. Jost[1], Olivia Laub[3,4], Juliana Drozd[1,5], Samuel L. Goldberg[1,6], Tyler Mackey[1,7], Fran Meyer[1,5], Athena Eyster[1,8]

[1]Department of Earth, Atmospheric and Planetary Sciences, Massachusetts Institute of Technology, Cambridge, MA 02139
[2]now at Department of Geosciences, Goethe-Universität
Frankfort, Germany
[3]Department of Geology, Carleton College
Northfield, MN 55057
[4]now at Geosciences Department, Utah State University
Logan, UT 84322
[5]now at Department of Geosciences, Pennsylvania State University
[6]now at Rosenstiel School of Marine and Atmospheric Science, University of Miami
Miami, FL 33149
[7]now at Department of Earth and Planetary Sciences, University of New Mexico
Albuquerque, NM 87131
State College, PA 16801
[8]now at Department of Geoscience, University of Wisconsin, Madison
Madison, WI 53706
[*]To whom correspondence should be addressed; E-mail: kdberg@mit.edu.

The habitability and ecology of Earth is fundamentally shaped by surface tem-

perature, but the temperature history of our planet is not easily reconstructed before the evolution of early biomineralizing animals. This work presents a billion year, high-resolution, mineral-specific record of oxygen isotope measurements in shallow marine rocks. Clumped-isotope paleothermometry results from four minerals resolves previous ambiguity with seawater oxygen isotope composition and confirms that long-term cooling punctuated by higher-frequency variations are dominant components of this record. We consider post-depositional effects by comparing Phanerozoic rock and fossil records, and identify temporal and spatial controls on alteration. Key differences in the dolomite oxygen isotope record exist between the Neoproterozoic (1000–538.8 Ma) and the Phanerozoic (538.8–0 Ma), suggesting a shift from proto-dolomite or primary dolomite to secondary dolomite formation processes. This record, when viewed alongside the fossil record, suggests temperature change is tightly coupled to extinction and origination in the history of life and carbon cycle perturbations over the last billion years.

One sentence summary: Earth's long-term temperature evolution, as recorded by oxygen isotopes in shallow marine rocks, shows that temperature was a key variable in the expansion of complex life.

Uncertainty in Earth's surface temperature through time To understand why complex life evolved on Earth—and to grasp how rare it may be in the Universe—we must identify and quantify the variables that have controlled habitability and permitted the emergence of complex life. The temperature of Earth's surface environments is a key control on modern ecosystems, yet it is poorly constrained in Earth's distant past. Quantifying Earth's surface temperature history in deep time ($\sim10^9$ y) will inform our understanding of the interplay between climate, carbon, and life on Earth.

For decades, consensus from models and data analysis has held (*1–4*) that average global temperatures in the deep past were similar to those observed in the Cenozoic (*5*). Previous efforts document a protracted increase towards the modern in the oxygen isotopic composition (δ^{18}O) of various minerals precipitated from seawater (e.g. calcite (*1, 2, 6*), apatite (*6, 7*), chert (*8, 9*), iron oxides (*3*)) and preserved in ancient marine sedimentary rocks. However, interpretations of this increases in mineral δ^{18}O are inherently equivocal because of a dependence on the temperature of precipitation, oxygen isotopic composition of seawater, and post-depositional alteration. This uncertainty has provoked a half-century of debate about the relative importance of long-term cooling, secular increase in seawater δ^{18}O values, or diagenetic alteration (*1–4, 7, 8*).

Carbonate clumped-isotope (Δ_{47}) thermometry has the potential to resolve this debate (*10*) and, when paired with petrography and constraints on burial history, yields insights into post-depositional alteration (i.e., (*11–13*)). The thermodynamic underpinning of clumped-isotope thermometry relies on the temperature-dependence of multiple substitutions of heavy isotopes within a given molecule independent of seawater oxygen isotope composition (*10*). In the absence of post-depositional alteration, seawater δ^{18}O values can be calculated from coupled measurements of Δ_{47}-temperature and mineral δ^{18}O values (*10*).

To build an improved record of Earth's temperature history, we must both quantify the competing effects of temperature and seawater oxygen isotope composition using clumped isotope thermometry, and contend with significant changes in the carbonate record over its 3.8 billion year history. These changes include a lack of open ocean and deep ocean records before $\sim$145 Ma (*14*) and coastal fossils prior to 538.8 Ma (*15*). A comprehensive, continuous carbonate oxygen isotope record will necessarily include samples that have been altered, that formed from environments with varying primary temperatures and water oxygen isotope values, and that reflect material-specific formation processes. This paper presents a time-resolved compilation of calcite and dolomite mineral δ^{18}O values spanning the last billion years in the context of Δ_{47}-temperature and Δ_{47}-derived water values. After exploring controls on δ^{18}O values and variability between materials, we develop an approach to minimize the effects of alteration and present an estimate of shallow marine temperature over the last billion years. Finally, we consider the implications of our results for Earth's habitability and the evolution of complex life.

Assessing temperature versus seawater oxygen isotope evolution in the Neoproterozoic
In total, our compilation includes 30,981 mineral δ^{18}O and 75 Δ_{47}-temperature values of limestone rocks and 5,574 mineral δ^{18}O and 128 Δ_{47}-temperature values of dolomite rocks (Fig. 1)(See SI for a complete reference list). This record is combined with 7,418 previously compiled mineral δ^{18}O values and 163 Δ_{47}-temperature measurements of calcite fossils (e.g., brachiopods and belemnites) from shallow nearshore environments and 71,452 δ^{18}O values from open ocean and deep sea planktonic and benthic foraminifera (*5, 11–13, 15–18*). All datasets use a consistent age model in the Phanerozoic (*19*) and Neoproterozoic (*20–22*).

Initially, we consider all mineral δ^{18}O and Δ_{47}-temperature values in the compilation, despite clear evidence for alteration in some samples. We explore the implications of two end-member interpretations of the long-standing paleoclimate debate using the mineral-specific functional dependence of seawater δ^{18}O values and temperature on mineral δ^{18}O values (*23–25*). In Scenario 1, we assume an invariant seawater $\delta^{18}O_{VSMOW}$ value of $-1.2‰$, an estimate of recent ice-free seawater δ^{18}O (*26, 27*), which we use to calculate the Gaussian kernel density estimate of temperature over time (*23–25*)(Fig. 2, thin line, left panels). In Scenario 2, we hold seawater temperature at a constant 25°C over the last 1.5 Ga, and use mineral δ^{18}O values to calculate the Gaussian kernel density estimate of seawater δ^{18}O values (*23–25*)(Fig. 2, thin line, right panels). This scenario predicts seawater $\delta^{18}O_{VSMOW}$ values with a mode of $-6‰$ in the Neoproterozoic as suggested by (*1, 2*)(Fig. 2). Post-depositional alteration generally lowers mineral δ^{18}O—leading to a right-skewed distribution in Scenario 1 and a left-skewed distribution in Scenario 2 (Fig. 2, thin lines).

To resolve Scenarios 1 and 2, we overlay Δ_{47}-temperature and Δ_{47}-derived seawater δ^{18}O values from five different materials (limestone (n = 75) and dolomite rocks (n = 128); a collection of all calcite, apatite and aragonite fossils (n = 163)) (*11–13, 16–18*)(Fig. 2, bold lines). The portion of overlap (η) between Gaussian kernel density estimates between each scenario (light lines) and Δ_{47} results (bold lines), is shaded (Fig. 2). There is significant overlap between Scenario 1 and the Δ_{47}-temperature population over the entire record. While there is overlap between Scenario 2 and Δ_{47}-derived water δ^{18}O values in the Phanerozoic fossil and limestone rock populations, there is little overlap with Scenario 2 in the Precambrian limestone and dolomite rock populations. Instead, the median of Δ_{47}-derived water δ^{18}O values indicate that shallowly buried carbonate rocks and fossils have lithified in the presence of fluids with $\delta^{18}O_{VSMOW}$ values similar to or greater than -1.2‰ for the last billion years (Fig. 2). Our results are compatible with an independent estimate of Neoproterozoic seawater $\delta^{18}O_{VSMOW}$ of $-1.33 \pm 0.98‰$ (*28*). A constant seawater composition over the last billion years of Earth's history is also consistent with ophiolite δ^{18}O datasets indicating that mid-ocean ridge buffering processes have not changed over this timescale (i.e., (*29, 30*)). Our results are inconsistent with interpretations of seawater oxygen isotope estimates from iron oxides in the Neoproterozoic, although iron oxide data is sparse (*3*).

Studies often document a range in Δ_{47}-temperatures from a given location and time interval, reflecting alteration and solid state reordering (*11–13, 16–18*)(right-skewed bold distributions in Fig. 2a,b,c). Petrographic and crystallographic observations show that the preservation of original carbonate fabric coincides with minimum Δ_{47}-temperatures and that visibly altered carbonates record elevated Δ_{47}-temperatures, except for in regions affected by solid state reordering. This suggests that the lowest Δ_{47}-temperatures record marine or shallow burial conditions (*11–13, 31*)(Fig. 2). Samples with elevated Δ_{47}-temperatures have apparent Δ_{47}-derived elevated seawater $\delta^{18}O_{VSMOW}$ values either reflecting sediment-buffered alteration or solid state reordering processes that do not reset mineral δ^{18}O values; this trend creates a right-skewed distribution (bold lines in Fig. 2c,d,e).

Time-dependent variability across materials We explore controls on variability in the δ^{18}O-derived temperature data in Scenario 1 by considering limestone, dolomite, coastal shallow marine fossils, open ocean and deep ocean fossil records individually and relative to each other both temporally and spatially (Fig. 3, Fig. S2). There is agreement in both distribution and variance between limestone and coastal fossils for many time periods in the Phanerozoic Era, particularly in the early Phanerozoic (Fig. 3b). The Late Paleozoic Ice Age (345–290 Ma) is one point of difference, likely because of the compounding effects of meteoric alteration on limestone from high amplitude sea level oscillation and a switch from calcite to aragonite as the dominant primary carbonate mineralogy (*32*)(Fig. 1,3). In the most recent portion of the record, the bulk limestone dataset is currently sparse as it is less common to report δ^{18}O values in publications—a sparse record can be more easily biased by alteration (Fig. 3a,b).

Compiling all available mineralogies in our database reveals the 'dolomite problem', the significant contribution dolomite makes to the carbonate record in the early Phanerozoic and Neoproterozoic compared to the recent (Fig. 1). Intriguingly, the Neoproterozoic limestone and dolomite records often overlap in temperature space, indicating they formed from the same fluid at the same temperature (Fig. 3b). This aligns well with petrographic and crystallographic evidence that Neoproterozoic dolomite formed on or near the seafloor as proto-dolomite or dolomite, and stabilized as dolomite in the shallow sediments without significant fluid-alteration (*33–35*). This temperature similarity does not hold for locations in the Neoproterozoic with lower limestone δ^{18}O values indicative of more deeply buried strata (Fig. S2). In contrast, early Phanerozoic dolomite is clearly 'hotter' under the Scenario 1 assumption (Fig. 3b). This distinction aligns well with petrographic evidence that early Phanerozoic dolomite is often fabric destructive and forms from fluid-buffered alteration at some point during burial (*17, 36*). Together these results indicate shallow marine Neoproterozoic environments were conducive to dolomite formation because of different physio-chemical parameters (i.e. high temperatures or high silica, etc.) (*33, 37*).

Temperature can be strongly coupled to the carbon cycle, through feedbacks with enhanced outgassing, organic matter remineralization, organic matter burial, terrestrial organic matter addition to marine environments, deep ocean outgassing, or methane clathrate destabilization (*38, 39*). Carbon cycle trends can in turn can impact the carbon isotopic composition of marine carbonates. We also assess the δ^{13}C variability across materials and mineralogies through time keeping both alteration and carbon cycle processes in mind. In general, the limestone record is even more similar to the coastal fossil record in δ^{13}C values than δ^{18}O values, in both distribution and variance, because carbon isotopes are more robust to alteration (Fig. 3c,d). While the δ^{13}C values of Neoproterozoic dolomite and limestone often diverge, we note the significant variability in the record itself during this time interval. Some large carbon isotope excursions have a temporal mineralogical signal across them (*40, 41*). Dolomite and limestone are often forming in shallow and deeper water environments in the Neoproterozoic, respectively (*35*). Their divergence may also reflect a water column depth gradient in δ^{13}C (*42*).

Constructing a long-term temperature record To minimize outliers from meteoric or burial alteration, we filter the dataset by only including the 5th to 50th quantiles of Scenario 1 temperature with a moving distribution and the 25^{th} to 75^{th} quantiles of δ^{13}C from limestone and shallow marine fossil data from the entire available record and dolomite data from the Neoproterozoic younger than 800 Ma (Fig. 3c,f). Despite setting data limits, this is a warm-biased temperature record because we can only sample past tropical, coastal environments in deeper time including higher temperature peritidal environments (*14*).

The Neoproterozoic experienced short intervals with hot coastal temperatures followed by long-term cooling including into Snowball-earth glaciations (*13*)(Fig. 4). The first third of the Phanerozoic is characterized by significant cooling from coastal equatorial temperatures near 40°C to ∼20°C. Climate events co-occur with δ^{13}C perturbations across the entire record (*38*). In periods with known glacial deposits (blue bars in Fig. 4), we observe cooler temperatures than surrounding rocks in agreement with published Δ_{47} studies (*12, 13, 18*)(Fig. 4). Carbonate rocks capturing the Sturtian 'Snowball earth' glaciation (660-717 Ma) (*43*) record some of the most enriched mineral δ^{18}O values in tropical environments over the last billion years, and thus the coldest extrapolated temperatures in Scenario 1 (Fig. 4) (*13*). Note that the temperatures are likely too cold because our first-order Scenario 1 assumption does not account for ice volume changes during glaciations.

We identify four potential sources of error for earliest Phanerozoic and Neoproterozoic temperature in the current approach: [1] shallow, coastal Precambrian dolomite might form in more evaporatively ^{18}O-enriched water, [2] Neoproterozoic oceans may have been dominated by aragonite precipitation similar to the Late Paleozoic, and thus are perhaps more susceptible to δ^{18}O alteration as a population, [3] Limestone and dolomite δ^{18}O mineral values may have been more prone to alteration before shells were a part of the carbonate depositional environment, [4] sparse sampling (e.g., the earliest Neoproterozoic, 1000–850 Ma). To account for these potential temperature offsets, more high-resolution paired δ^{18}O and Δ_{47}-temperature studies are necessary from well-preserved rocks in the Neoproterozoic.

Out of the twilight zone and into the tropics Life remained microscopic for at least three billion years of Earth's history. Life rapidly explores its fitness landscape, so this size restriction suggests that formidable evolutionary pressures kept life small. The hypothesis that low dissolved oxygen concentrations was the dominant environmental parameter keeping Precambrian life microscopic and single-celled (*44*) has limitations (*45*). For example, marine oxygen concentrations were likely spatially variable following the Great Oxidation Event as evidenced by proxy variability (i.e., (*46*)). Furthermore, modern observations and experiments indicate that some macroscopic animals can grow in exceedingly low oxygen conditions (*47*).

Our temperature record in the Neoproterozoic and early Phanerozoic—the interval of time when complex, multicellular, macroscopic life evolved and thrived—is punctuated by higher-frequency temperature variations suggesting that temperature was a key control on the emergence and early evolutionary patterns of complex life (*45, 48, 49*). We present extinction and origination intensities (%) for the Phanerozoic (*50*) and estimate them in the Neoproterozoic for microscopic fossil populations (*51–53*) and macroscopic Ediacaran fauna (*54*)(Fig. 4). In the Phanerozoic, temperature increases are often associated with increased rates of extinction following by increased intensity of origination (*55*); this pattern is particularly true in the early Cambrian (Fig. 4). In the Neoproterozoic, high temperature events—evidenced by negative carbon isotope excursions like the mid-Ediacaran Shuram excursion and Bitter Springs excursions—were extinction events for nascent complex life (*40*)(Fig. 4). As silicate weathering cooled the climate in response to the initial perturbation (*4*), periods of cooler temperatures and increased dissolved oxygen in the oceans allowed for innovation and origination.

Support for the controlling effect of temperature—both the longer-term cooling and rapid shifts to elevated temperatures—on Earth's habitability through time comes from the fossil record in four forms: [1] in the modern, high temperature environments limit the size of both larvae and adult ectotherms and endotherms, providing one potential control on the microscopic body size of almost all taxa in the Precambrian (see (*49*)), [2] Macroscopic Ediacaran fauna appear first in deep water refugia, which likely experienced less temperature variability (*45,48,49*); the first shallow water Ediacaran fossils appear after a 20-million year lag appear to go extinct coincident with a temperature increase in shallow marine carbonates(Fig. 4), [3] significant eukaryotic lagerstätte, both microscopic and macroscopic appear in the strata between large negative carbon isotope and temperature anomalies (*20, 21, 45, 51, 53, 56*)(Fig. 4), and [4] extinction intensity (%) is elevated during high temperature perturbations (i.e., portions of the Cambrian) and origination intensity (%) is high in their cooling aftermath (Fig. 4)(See Methods). The long-term cooling may reflect periods of enhanced carbon sequestration, first into carbonate rocks on continental crust in the early Paleozoic (*57*), later after land plant evolution (*58*), and finally associated with the evolution of planktonic biomineralizing organisms in the Cretaceous and Cenozoic (*59, 60*)(Fig. 4). Our record suggests that by the second half of the Phanerozoic equatorial sea surface temperatures remained below extinction thresholds for many macroscopic, complex animals even during climate perturbations, providing a mechanism for the observed decrease in extinction and origination intensities over the Phanerozoic (*61*). The Cambrian and early Ordovician peak in extinction and origination intensities was previously poorly linked to environmental change (*46*). Our record identifies intervals in the Neoproterozoic and early Phanerozoic when shallow marine environments would have experienced changing dissolved oxygen concentrations because O_2 solubility is temperature-dependant (*48*).

Conclusions Pairing clumped-isotope thermometry and a data-rich oxygen isotope compilation reveals that temperature change, not seawater oxygen isotope evolution, is the primary driver of the long term increase in the oxygen isotope composition of carbonate rocks over the last billion years. Our results suggest that well-documented Cenozoic cooling (*5*) pales in comparison to the cooling in Earth's more distant past. On a finer scale, the record captures cooling and warming associated with known glacial-greenhouse transitions. Our record suggests long-held beliefs about the fallibility of the oxygen isotopic composition of carbonate rocks can be overcome with large, global compilations. We also find evidence for dolomite formation on the seafloor or in the shallowest sediments in the Neoproterozoic. Our record also suggests decreasing volatility of both the carbon cycle and climate system through time in line with extinction and origination rates, and that hot episodes were bottlenecks for early complex life. Comparisons to the fossil record suggest cooling following coupled climate-carbon cycle perturbations allowed for origination and diversification, and volatility was critical for enhancing turnover rates and clearing the evolutionary landscape.

Acknowledgements K.D.B. is grateful to Andy Knoll for providing a sample suite analyzed in this study from many of his field sites. K.D.B. thanks Clint Cowan for providing comments on early drafts of this work and for being a sounding board for ideas.

Funding M.D.C. was supported by a National Defense Science and Engineering Graduate Fellowship. K.D.B. acknowledges funding from the Packard Foundation and NASA Exobiology Grant 80NSSC19K0464. Research was conducted and permitted under the Research in Svalbard (RIS) ID 6867.

Author Contributions K.D.B. conceptualized the study, developed the methodology, and wrote the original draft. N.B. and K.D.B contributed software, formal analysis and visualization. K.D.B, J.W.C., J.D., and O.L. contributed data curation. K.D.B, J.W., and N.T.A. supervised data curation. All authors reviewed and edited the manuscript.

Data and materials availability All data are provided in the supplementary materials. Upon manuscript acceptance, unpublished data, figures and code will be made available on Open Science Framework (link).

Supplementary Materials :

Materials and Methods

Figs. S1 - S2

References (59 - 177)

References and Notes

1. J. Veizer, P. Bruckschen, F. Pawellek, A. Diener, O. G. Podlaha, G. A. F. Carden, T. Jasper, C. Korte, H. Strauss, K. Azmy, D. Ala, Oxygen isotope evolution of Phanerozoic seawater. *Palaeogeogr. Palaeoclimatol. Palaeoecol.* **132**, 159–172 (1997).

2. J. B. D. Jaffrés, G. A. Shields, K. Wallmann, The oxygen isotope evolution of seawater: A critical review of a long-standing controversy and an improved geological water cycle model for the past 3.4 billion years. *Earth-Science Rev.* **83**, 83–122 (2007).

3. N. Galili, A. Shemesh, R. Yam, I. Brailovsky, M. Sela-Adler, E. M. Schuster, C. Collom, A. Bekker, N. Planavsky, F. A. Macdonald, A. Préat, M. Rudmin, W. Trela, U. Sturesson, J. M. Heikoop, M. Aurell, J. Ramajo, I. Halevy, The geologic history of seawater oxygen isotopes from marine iron oxides. *Science (80-.).* **365**, 469–473 (2019).

4. J. C. G. Walker, P. B. Hays, J. F. Kasting, A negative feedback mechanism for the long-term stabilization of Earth's surface temperature. *J. Geophys. Res. Ocean.* **86**, 9776–9782 (1981).

5. T. Westerhold, N. Marwan, A. J. Drury, D. Liebrand, C. Agnini, E. Anagnostou, J. S. K. Barnet, S. M. Bohaty, D. De Vleeschouwer, F. Florindo, T. Frederichs, D. A. Hodell, A. E. Holbourn, D. Kroon, V. Lauretano, K. Littler, L. J. Lourens, M. Lyle, H. Pälike, U. Röhl, J. Tian, R. H. Wilkens, P. A. Wilson, J. C. Zachos, An astronomically dated record of Earth's climate and its predictability over the last 66 million years. *Science (80-.).* **369**, 1383–1387 (2020).

6. E. L. Grossman, M. M. Joachimski, Ocean temperatures through the phanerozoic re-assessed. *Scientific Reports* **12**, 1–13 (2022).

7. J. A. Trotter, I. S. Williams, C. R. Barnes, C. Lécuyer, R. S. Nicoll, Did cooling oceans trigger Ordovician biodiversification? Evidence from conodont thermometry. *Science* **321**, 550–554 (2008).

8. L. P. Knauth, D. R. Lowe, High Archean climatic temperature inferred from oxygen isotope geochemistry of cherts in the 3.5 Ga Swaziland Supergroup, South Africa. *Bull. Geol. Soc. Am.* **115**, 566–580 (2003).

9. F. Robert, M. Chaussidon, A palaeotemperature curve for the Precambrian oceans based on silicon isotopes in cherts. *Nature* **443**, 969–972 (2006).

10. J. M. Eiler, "Clumped-isotope" geochemistry-The study of naturally-occurring, multiply-substituted isotopologues. *Earth Planet. Sci. Lett.* **262**, 309–327 (2007).

11. K. D. Bergmann, S. Finnegan, R. Creel, J. M. Eiler, N. C. Hughes, L. E. Popov, W. W. Fischer, A paired apatite and calcite clumped isotope thermometry approach to estimat-

ing Cambro-Ordovician seawater temperatures and isotopic composition. *Geochim. Cosmochim. Acta* **224**, 18–41 (2018).

12. K. D. Bergmann, S. A. Al Balushi, T. J. MacKey, J. P. Grotzinger, J. M. Eiler, A 600-million-year carbonate clumped-isotope record from the Sultanate of Oman. *J. Sediment. Res.* **88**, 960–979 (2018).

13. T. J. Mackey, A. B. Jost, J. R. Creveling, K. D. Bergmann, A decrease to low carbonate clumped isotope temperatures in Cryogenian strata. *AGU Adv.* **1** (2020).

14. E. J. Judd, T. Bhattacharya, L. C. Ivany, A Dynamical Framework for Interpreting Ancient Sea Surface Temperatures. *Geophys. Res. Lett.* **47** (2020).

15. E. Grossman, M. Joachimski, Oxygen isotope stratigraphy. *Geologic Time Scale 2020* (Elsevier, 2020), pp. 279–307.

16. G. A. Henkes, B. H. Passey, E. L. Grossman, B. J. Shenton, T. E. Yancey, A. Pérez-Huerta, Temperature evolution and the oxygen isotope composition of Phanerozoic oceans from carbonate clumped isotope thermometry. *Earth Planet. Sci. Lett.* **490**, 40–50 (2018).

17. U. Ryb, J. M. Eiler, Oxygen isotope composition of the Phanerozoic ocean and a possible solution to the dolomite problem. *Proc. Natl. Acad. Sci. U. S. A.* **115**, 6602–6607 (2018).

18. S. Finnegan, K. Bergmann, J. Eiler, D. Jones, D. Fike, I. Eisenman, N. Hughes, A. Tripati, W. Fischer, The magnitude and duration of late Ordovician-early Silurian glaciation. *Science (80-.).* **331** (2011).

19. F. M. Gradstein, J. G. Ogg, M. D. Schmitz, G. M. Ogg, *Geologic time scale 2020* (Elsevier, 2020).

20. A. D. Rooney, M. D. Cantine, K. D. Bergmann, I. Gómez-Pérez, B. A. Baloushi, T. H. Boag, J. F. Busch, E. A. Sperling, J. V. Strauss, Calibrating the coevolution of Ediacaran life and environment. *Proc. Natl. Acad. Sci. U. S. A.* **117**, 16824–16830 (2020).

21. C. Yang, A. D. Rooney, D. J. Condon, X.-H. Li, D. V. Grazhdankin, F. T. Bowyer, C. Hu, F. A. Macdonald, M. Zhu, The tempo of Ediacaran evolution. *Science advances* **7**, eabi9643 (2021).

22. Y. Park, N. L. Swanson-Hysell, S. A. MacLennan, A. C. Maloof, M. Gebreslassie, M. M. Tremblay, B. Schoene, M. Alene, E. S. Anttila, T. Tesema, B. Haileab, The lead-up to the Sturtian Snowball Earth: Neoproterozoic chemostratigraphy time-calibrated by the Tambien Group of Ethiopia. *GSA Bull.* **132**, 1119–1149 (2020).

23. S. T. Kim, J. R. O'Neil, Equilibrium and nonequilibrium oxygen isotope effects in synthetic carbonates. *Geochim. Cosmochim. Acta* **61**, 3461–3475 (1997).

24. J. Horita, Oxygen and carbon isotope fractionation in the system dolomite–water–CO2 to elevated temperatures. *Geochim. Cosmochim. Acta* **129**, 111–124 (2014).

25. S. T. Kim, J. R. O'Neil, C. Hillaire-Marcel, A. Mucci, Oxygen isotope fractionation between synthetic aragonite and water: Influence of temperature and Mg2+ concentration. *Geochim. Cosmochim. Acta* **71**, 4704–4715 (2007).

26. C. H. Lear, Cenozoic Deep-Sea Temperatures and Global Ice Volumes from Mg/Ca in Benthic Foraminiferal Calcite. *Science (80-.).* **287**, 269–272 (2000).

27. B. S. Cramer, K. G. Miller, P. J. Barrett, J. D. Wright, Late Cretaceous-Neogene trends in deep ocean temperature and continental ice volume: Reconciling records of benthic foraminiferal geochemistry (δ18O and Mg/Ca) with sea level history. *J. Geophys. Res. Ocean.* **116**, C12023 (2011).

28. F. Hodel, M. Macouin, R. I. F. Trindade, A. Triantafyllou, J. Ganne, V. Chavagnac, J. Berger, M. Rospabé, C. Destrigneville, J. Carlut, N. Ennih, P. Agrinier, Fossil black smoker yields oxygen isotopic composition of Neoproterozoic seawater. *Nat. Commun.* **9**, 1453 (2018).

29. K. Muehlenbachs, R. N. Clayton, Oxygen isotope composition of the oceanic crust and its bearing on seawater. *J. Geophys. Res.* **81**, 4365–4369 (1976).

30. C. Holmden, K. Muehlenbachs, The 18O/16O Ratio of 2-Billion-Year-Old Seawater Inferred from Ancient Oceanic Crust. *Science* **259**, 1733–6 (1993).

31. P. Gilbert, K. Bergmann, C. Myers, M. Marcus, R. DeVol, C.-Y. Sun, A. Blonsky, E. Tamre, J. Zhao, E. Karan, N. Tamura, S. Lemer, A. Giuffre, G. Giribet, J. Eiler, A. Knoll, Nacre tablet thickness records formation temperature in modern and fossil shells. *Earth Planet. Sci. Lett.* **460** (2017).

32. J. B. Ries, Review: geological and experimental evidence for secular variation in seawater Mg/Ca (calcite-aragonite seas) and its effects on marine biological calcification. *Biogeosciences* **7**, 2795–2849 (2010).

33. J. Wilcots, P. Gilbert, K. Bergmann, Nanoscale crystal fabric preserved in dolomite ooids at the onset of the ediacaran shuram excursion. *Geophysical Research Letters* (PrePrint).

34. M. E. Tucker, Precambrian dolomites: petrographic and isotopic evidence that they differ from Phanerozoic dolomites. *Geology* **10**, 7–12 (1982).

35. M. D. Cantine, A. H. Knoll, K. D. Bergmann, Carbonates before skeletons: A database approach. *Earth-Science Reviews* **201**, 103065 (2020).

36. F. A. Corsetti, D. L. Kidder, P. J. Marenco, Trends in oolite dolomitization across the Neoproterozoic-Cambrian boundary: A case study from Death Valley, California. *Sediment. Geol.* **191**, 135–150 (2006).

37. Y. Fang, H. Xu, Dissolved silica-catalyzed disordered dolomite precipitation. *American Mineralogist: Journal of Earth and Planetary Materials* **107**, 443–452 (2022).

38. S. M. Stanley, Relation of Phanerozoic stable isotope excursions to climate, bacterial metabolism, and major extinctions. *Proc. Natl. Acad. Sci. U. S. A.* **107**, 19185–19189 (2010).

39. S. K. Turner, Pliocene switch in orbital-scale carbon cycle/climate dynamics. *Paleoceanography* **29**, 1256–1266 (2014).

40. K. D. Bergmann, M. R. Osburn, J. Wilcots, M. D. Cantine, J. P. Grotzinger, W. W. Fischer, J. M. Eiler, M. Bonifacie, The shuram excursion: A response to climate extremes at the dawn of animal life. *Preprint at 10.1002/essoar.10511917.1* (2022).

41. J. F. Busch, E. B. Hodgin, A.-S. C. Ahm, J. M. Husson, F. A. Macdonald, K. D. Bergmann, J. A. Higgins, J. V. Strauss, Global and local drivers of the ediacaran shuram carbon isotope excursion. *Earth and Planetary Science Letters* **579**, 117368 (2022).

42. G. Jiang, A. J. Kaufman, N. Christie-Blick, S. Zhang, H. Wu, Carbon isotope variability across the Ediacaran Yangtze platform in South China: Implications for a large surface-to-deep ocean δ^{13}C gradient. *Earth Planet. Sci. Lett.* **261**, 303–320 (2007).

43. A. D. Rooney, J. V. Strauss, A. D. Brandon, F. A. Macdonald, A Cryogenian chronology: Two long-lasting synchronous neoproterozoic glaciations. *Geology* **43**, 459–462 (2015).

44. T. W. Lyons, C. T. Reinhard, N. J. Planavsky, The rise of oxygen in Earth's early ocean and atmosphere. *Nature* **506**, 307–15 (2014).

45. F. Zhang, H. Wang, Y. Ye, Y. Liu, Y. Lyu, Y. Deng, D. Lyu, X. Wang, H. Wu, S. Deng, *et al.*, Did high temperature rather than low o2 hinder the evolution of eukaryotes in the precambrian? *Precambrian Research* **378**, 106755 (2022).

46. E. A. Sperling, C. A. Frieder, A. V. Raman, P. R. Girguis, L. A. Levin, A. H. Knoll, Oxygen, ecology, and the Cambrian radiation of animals. *Proc. Natl. Acad. Sci. U. S. A.* **110**, 13446–51 (2013).

47. D. B. Mills, L. M. Ward, C. Jones, B. Sweeten, M. Forth, A. H. Treusch, D. E. Canfield, Oxygen requirements of the earliest animals. *Proceedings of the National Academy of Sciences* **111**, 4168–4172 (2014).

48. T. H. Boag, R. G. Stockey, L. E. Elder, P. M. Hull, E. A. Sperling, Oxygen, temperature and the deep-marine stenothermal cradle of Ediacaran evolution. *Proc. R. Soc. B Biol. Sci.* **285**, 20181724 (2018).

49. C. Simpson, Adaptation to a viscous snowball earth ocean as a path to complex multicellularity. *The American Naturalist* **198**, 590–609 (2021).

50. R. A. Rohde, R. A. Muller, Cycles in fossil diversity. *Nature* **434**, 208–210 (2005).

51. K. A. McFadden, J. Huang, X. Chu, G. Jiang, A. J. Kaufman, C. Zhou, X. Yuan, S. Xiao, Pulsed oxidation and biological evolution in the Ediacaran Doushantuo Formation. *Proc. Natl. Acad. Sci.* **105**, 3197–3202 (2008).

52. L. A. Riedman, S. M. Porter, C. R. Calver, Vase-shaped microfossil biostratigraphy with new data from Tasmania, Svalbard, Greenland, Sweden and the Yukon (2018).

53. S. Xiao, B. Shen, Q. Tang, A. J. Kaufman, X. Yuan, J. Li, M. Qian, Biostratigraphic and chemostratigraphic constraints on the age of early Neoproterozoic carbonate successions in North China. *Precambrian Res.* **246**, 208–225 (2014).

54. T. H. Boag, S. A. Darroch, M. Laflamme, Ediacaran distributions in space and time: Testing assemblage concepts of earliest macroscopic body fossils. *Paleobiology* **42**, 574–594 (2016).

55. H. Song, D. B. Kemp, L. Tian, D. Chu, H. Song, X. Dai, Thresholds of temperature change for mass extinctions. *Nature communications* **12**, 1–8 (2021).

56. L. A. Riedman, P. M. Sadler, Global species richness record and biostratigraphic potential of early to middle Neoproterozoic eukaryote fossils. *Precambrian Res.* **319**, 6–18 (2018).

57. K. D. Bergmann, J. Wilcots, T. Pico, N. Boekelheide, N. T. Anderson, M. D. Cantine, S. L. Goldberg, B. Keller, A. B. Jost, A. Eyster, Onset of carbonate biomineralization drove global reorganization of sedimentation and subsidence patterns. *Preprint at 10.1002/essoar.10511913.1* (2022).

58. T. W. Dahl, S. K. Arens, The impacts of land plant evolution on Earth's climate and oxygenation state–An interdisciplinary review. *Chemical Geology* **547**, 119665 (2020).

59. A. Ridgwell, R. E. Zeebe, The role of the global carbonate cycle in the regulation and evolution of the Earth system. *Earth Planet. Sci. Lett.* **234**, 299–315 (2005).

60. J. M. Edmond, Y. Huh, Non-steady state carbonate recycling and implications for the evolution of atmospheric pCO_2. *Earth Planet. Sci. Lett.* **216**, 125–139 (2003).

61. J. Alroy, M. Aberhan, D. J. Bottjer, M. Foote, F. T. Fürsich, P. J. Harries, A. J. Hendy, S. M. Holland, L. C. Ivany, W. Kiessling, M. A. Kosnik, C. R. Marshall, A. J. McGowan,

A. I. Miller, T. D. Olszewski, M. E. Patzkowsky, S. E. Peters, L. Villier, P. J. Wagner, N. Bonuso, P. S. Borkow, B. Brenneis, M. E. Clapham, L. M. Fall, C. A. Ferguson, V. L. Hanson, A. Z. Krug, K. M. Layou, E. H. Leckey, S. Nürnberg, C. M. Powers, J. A. Sessa, C. Simpson, A. Tomašových, C. C. Visaggi, Phanerozoic trends in the global diversity of marine invertebrates. *Science (80-.).* **321**, 97–100 (2008).

62. K. D. T. Nguyen, S. A. Morley, C. H. Lai, M. S. Clark, K. S. Tan, A. E. Bates, L. S. Peck, Upper temperature limits of tropical marine ectotherms: Global warming implications. *PLoS One* **6** (2011).

63. A. H. Knoll, A. J. Kaufman, M. A. Semikhatov, The carbon-isotopic composition of Proterozoic carbonates: Riphean successions from northwestern Siberia (Anabar Massif, Turukhansk uplift). *Am. J. Sci.* **295**, 823–850 (1995).

64. A. H. Knoll, R. K. Bambach, D. E. Canfield, J. P. Grotzinger, Comparative Earth history and Late Permian mass extinction. *Science (80-.).* **273**, 452–457 (1996).

65. L. C. Kah, A. G. Sherman, G. M. Narbonne, A. H. Knoll, A. J. Kaufman, δ ¹³ C stratigraphy of the Proterozoic Bylot Supergroup, Baffin Island, Canada: implications for regional lithostratigraphic correlations. *Can. J. Earth Sci.* **36**, 313–332 (1999).

66. G. J. Gilleaudeau, L. C. Kah, Carbon isotope records in a Mesoproterozoic epicratonic sea: Carbon cycling in a low-oxygen world. *Precambrian Res.* **228**, 85–101 (2013).

67. L. C. Kah, J. K. Bartley, D. A. Teal, Chemostratigraphy of the Late Mesoproterozoic Atar Group, Taoudeni Basin, Mauritania: Muted isotopic variability, facies correlation, and global isotopic trends. *Precambrian Res.* **200-203**, 82–103 (2012).

68. H. Guo, Y. Du, L. C. Kah, J. Huang, C. Hu, H. Huang, W. Yu, Isotopic composition of organic and inorganic carbon from the Mesoproterozoic Jixian Group, North China: Implications for biological and oceanic evolution. *Precambrian Res.* **224**, 169–183 (2013).

69. Y. Sawaki, T. Ohno, M. Tahata, T. Komiya, T. Hirata, S. Maruyama, B. F. Windley, J. Han, D. Shu, Y. Li, The Ediacaran radiogenic Sr isotope excursion in the Doushantuo Formation in the Three Gorges area, South China. *Precambrian Res.* **176**, 46–64 (2010).

70. D. A. Fike, J. P. Grotzinger, L. M. Pratt, R. E. Summons, Oxidation of the Ediacaran ocean. *Nature* **444**, 744–747 (2006).

71. M. R. Osburn, J. Owens, K. D. Bergmann, T. W. Lyons, Dynamic changes in sulfate sulfur isotopes preceding the Ediacaran Shuram Excursion. *Geochim. Cosmochim. Acta* (2015).

72. G. Jiang, X. Wang, X. Shi, S. Xiao, S. Zhang, J. Dong, The origin of decoupled carbonate and organic carbon isotope signatures in the early Cambrian (ca. 542-520Ma) Yangtze platform. *Earth Planet. Sci. Lett.* **317-318**, 96–110 (2012).

73. C. Lee, G. D. Love, W. W. Fischer, J. P. Grotzinger, G. P. Halverson, Marine organic matter cycling during the Ediacaran Shuram excursion. *Geology* **43**, 1103–1106 (2015).

74. C. Li, D. S. Hardisty, G. Luo, J. Huang, T. J. Algeo, M. Cheng, W. Shi, Z. An, J. Tong, S. Xie, N. Jiao, T. W. Lyons, Uncovering the spatial heterogeneity of Ediacaran carbon cycling. *Geobiology* **15**, 211–224 (2017).

75. B. G. Pokrovskii, V. A. Melezhik, M. I. Bujakaite, Carbon, oxygen, strontium, and sulfur isotopic compositions in late Precambrian rocks of the Patom Complex, central Siberia: Communication 1. results, isotope stratigraphy, and dating problems. *Lithol. Miner. Resour.* **41**, 450–474 (2006).

76. M. Tahata, Y. Ueno, T. Ishikawa, Y. Sawaki, K. Murakami, J. Han, D. Shu, Y. Li, J. Guo, N. Yoshida, T. Komiya, Carbon and oxygen isotope chemostratigraphies of the Yangtze platform, South China: Decoding temperature and environmental changes through the Ediacaran. *Gondwana Res.* **23**, 333–353 (2013).

77. X. Wang, G. Jiang, X. Shi, S. Xiao, Paired carbonate and organic carbon isotope variations of the Ediacaran Doushantuo Formation from an upper slope section at Siduping, South China. *Precambrian Res.* **273**, 53–66 (2016).

78. T. Ishikawa, Y. Ueno, T. Komiya, Y. Sawaki, J. Han, D. Shu, Y. Li, S. Maruyama, N. Yoshida, Carbon isotope chemostratigraphy of a Precambrian/Cambrian boundary section in the Three Gorge area, South China: Prominent global-scale isotope excursions just before the Cambrian Explosion. *Gondwana Res.* **14**, 193–208 (2008).

79. R. Kikumoto, M. Tahata, M. Nishizawa, Y. Sawaki, S. Maruyama, D. Shu, J. Han, T. Komiya, K. Takai, Y. Ueno, Nitrogen isotope chemostratigraphy of the Ediacaran and Early Cambrian platform sequence at Three Gorges, South China. *Gondwana Res.* **25**, 1057–1069 (2014).

80. G. M. Cox, G. P. Halverson, A. Poirier, D. Le Heron, J. V. Strauss, R. Stevenson, A model for Cryogenian iron formation. *Earth Planet. Sci. Lett.* **433**, 280–292 (2016).

81. G. P. Halverson, A. C. Maloof, P. F. Hoffman, The Marinoan glaciation (Neoproterozoic) in northeast Svalbard. *Basin Res.* **16**, 297–324 (2004).

82. G. P. Halverson, P. F. Hoffman, D. P. Schrag, A. J. Kaufman, A major perturbation of the carbon cycle before the Ghaub glaciation (Neoproterozoic) in Namibia: Prelude to snowball Earth? *Geochemistry, Geophys. Geosystems* **3**, 1–24 (2002).

83. G. P. Halverson, P. F. Hoffman, D. P. Schrag, A. C. Maloof, A. H. N. Rice, Toward a Neoproterozoic composite carbon-isotope record. *Bull. Geol. Soc. Am.* **117**, 1181–1207 (2005).

84. G. P. Halverson, A. C. Maloof, D. P. Schrag, F. Ö. Dudás, M. Hurtgen, Stratigraphy and geochemistry of a ca 800 Ma negative carbon isotope interval in northeastern Svalbard. *Chem. Geol.* **237**, 23–45 (2007).

85. D. T. Johnston, F. A. Macdonald, B. C. Gill, P. F. Hoffman, D. P. Schrag, Uncovering the Neoproterozoic carbon cycle. *Nature* **483** (2012).

86. A. B. Kuznetsov, M. A. Semikhatov, A. V. Maslov, I. M. Gorokhov, E. M. Prasolov, M. T. Krupenin, I. V. Kislova, New data on Sr-and C-isotopic chemostratigraphy of the Upper Riphean type section (southern Urals). *Stratigr. Geol. Correl.* **14**, 602–628 (2006).

87. N. L. Swanson-Hysell, C. V. Rose, C. C. Calmet, G. P. Halverson, M. T. Hurtgen, A. C. Maloof, Cryogenian glaciation and the onset of carbon-isotope decoupling. *Science (80-.).* **328**, 608–611 (2010).

88. H. Bao, I. J. Fairchild, P. M. Wynn, C. Spötl, Stretching the envelope of past surface environments: Neoproterozoic glacial lakes from Svalbard. *Science (80-.).* **323**, 119–122 (2009).

89. A.-S. C. Ahm, C. J. Bjerrum, P. F. Hoffman, F. A. Macdonald, A. C. Maloof, C. V. Rose, J. V. Strauss, J. A. Higgins, The ca and mg isotope record of the cryogenian trezona carbon isotope excursion. *Earth and Planetary Science Letters* **568**, 117002 (2021).

90. P. C. Boggiani, C. Gaucher, A. N. Sial, M. Babinski, C. M. Simon, C. Riccomini, V. P. Ferreira, T. R. Fairchild, Chemostratigraphy of the Tamengo Formation (Corumbá Group,

Brazil): A contribution to the calibration of the Ediacaran carbon-isotope curve. *Precambrian Res.* **182**, 382–401 (2010).

91. F. J. Gomez, N. Ogle, R. A. Astini, R. M. Kalin, Paleoenvironmental and carbon-oxygen isotope record of Middle Cambrian carbonates (La Laja Formation) in the Argentine Precordillera. *J. Sediment. Res.* **77**, 826–842 (2007).

92. R. A. Howley, G. Jiang, The Cambrian Drumian carbon isotope excursion (DICE) in the Great Basin, western United States. *Palaeogeogr. Palaeoclimatol. Palaeoecol.* **296**, 138–150 (2010).

93. A. C. Maloof, S. M. Porter, J. L. Moore, F. Ö. Dudás, S. A. Bowring, J. A. Higgins, D. A. Fike, M. P. Eddy, The earliest Cambrian record of animals and ocean geochemical change. *Bull. Geol. Soc. Am.* **122**, 1731–1774 (2010).

94. A. N. Sial, S. Peralta, V. P. Ferreira, A. J. Toselli, F. G. Aceñolaza, M. A. Parada, C. Gaucher, R. N. Alonso, M. M. Pimentel, Upper Cambrian carbonate sequences of the Argentine Precordillera and the Steptoean C-Isotope positive excursion (SPICE). *Gondwana Res.* **13**, 437–452 (2008).

95. E. F. Smith, F. A. Macdonald, T. A. Petach, U. Bold, D. P. Schrag, Integrated stratigraphic, geochemical, and paleontological late Ediacaran to early Cambrian records from southwestern Mongolias. *Bull. Geol. Soc. Am.* **128**, 442–468 (2016).

96. C. K. Thompson, L. C. Kah, Sulfur isotope evidence for widespread euxinia and a fluctuating oxycline in Early to Middle Ordovician greenhouse oceans. *Palaeogeogr. Palaeoclimatol. Palaeoecol.* **313-314**, 189–214 (2012).

97. S. J. Loyd, P. J. Marenco, J. W. Hagadorn, T. W. Lyons, A. J. Kaufman, F. Sour-Tovar, F. A. Corsetti, Sustained low marine sulfate concentrations from the Neoproterozoic to

the Cambrian: Insights from carbonates of northwestern Mexico and eastern California. *Earth Planet. Sci. Lett.* **339-340**, 79–94 (2012).

98. L. A. Derry, M. D. Brasier, R. M. Corfield, A. Y. Rozanov, A. Y. Zhuravlev, Sr and C isotopes in Lower Cambrian carbonates from the Siberian craton: A paleoenvironmental record during the 'Cambrian explosion'. *Earth Planet. Sci. Lett.* **128**, 671–681 (1994).

99. C. Chang, W. Hu, X. Wang, H. Yu, A. Yang, J. Cao, S. Yao, Carbon isotope stratigraphy of the lower to middle cambrian on the eastern yangtze platform, south china. *Palaeogeography, Palaeoclimatology, Palaeoecology* **479**, 90–101 (2017).

100. L. Ainsaar, D. Kaljo, T. Martma, T. Meidla, P. Männik, J. Nõlvak, O. Tinn, Middle and Upper Ordovician carbon isotope chemostratigraphy in Baltoscandia: A correlation standard and clues to environmental history. *Palaeogeogr. Palaeoclimatol. Palaeoecol.* **294**, 189–201 (2010).

101. K. Azmy, I. Knight, D. Lavoie, G. Chi, Origin of dolomites in the Boat Harbour Formation, St. George Group, in western Newfoundland, Canada: Implications for porosity development. *Bull. Can. Pet. Geol.* **57**, 81–104 (2009).

102. K. Lynn Batten Hender, Mixed Siliciclastic-Carbonate ramp sediments and coral bioherms of the Late Ordovician Lourdes Formation, Western Newfoundland: Sedimentology, Stratigraphy, and Tectonic Significance, Ph.D. thesis, Carleton University (2007).

103. P. a. Brandl, Carbon and oxygen isotopes, stratigraphy, and facies of the Oslobreen Group (northeast Ny Friesland, Svalbard), Ph.D. thesis (2009).

104. C. T. Edwards, M. Saltzman, Paired carbon isotopic analysis of Ordovician bulk carbonate (δ13Ccarb) and organic matter (δ13Corg) spanning the Great Ordovician Biodiversification Event. *Palaeogeogr. Palaeoclimatol. Palaeoecol.* **458**, 102–117 (2016).

105. A. Husinec, S. M. Bergström, Stable carbon-isotope record of shallow-marine evaporative epicratonic basin carbonates, Ordovician Williston Basin, North America. *Sedimentology* **62**, 314–349 (2015).

106. D. Kaljo, L. Hints, T. Martma, J. Nõlvak, A. Oraspõld, Late Ordovician carbon isotope trend in Estonia, its significance in stratigraphy and environmental analysis. *Palaeogeogr. Palaeoclimatol. Palaeoecol.* **210**, 165–185 (2004).

107. A. Lindskog, A. M. L. Lindskog, J. V. Johansson, P. Ahlberg, M. E. Eriksson, H. Smithsgatan, The Cambrian-Ordovician succession at Lanna, Sweden: stratigraphy and depositional environments. *Est. J. Earth Sci.* **67**, 133–148 (2018).

108. A. Mauviel, A. Desrochers, A high-resolution, continuous δ13C record spanning the ordovician-silurian boundary on Anticosti Island, Eastern Canada. *Can. J. Earth Sci.* **53**, 795–801 (2016).

109. P. McLaughlin, P. Emsbo, A. Desrochers, A. Bancroft, C. Brett, J. Riva, W. Premo, L. Neymark, A. Achab, E. Asselin, M. Emmons, Refining 2 km of ordovician chronostratigraphy beneath anticosti island utilizing integrated chemostratigraphy. *Can. J. Earth Sci.* **53**, 1–10 (2016).

110. P. C. Quinton, A. D. Herrmann, S. A. Leslie, K. G. MacLeod, Carbon cycling across the southern margin of Laurentia during the Late Ordovician. *Palaeogeogr. Palaeoclimatol. Palaeoecol.* **458**, 63–76 (2016).

111. C. M. Ø. Rasmussen, C. V. Ullmann, K. G. Jakobsen, A. Lindskog, J. Hansen, T. Hansen, M. E. Eriksson, A. Dronov, R. Frei, C. Korte, A. T. Nielsen, D. A. Harper, Onset of main Phanerozoic marine radiation sparked by emerging Mid Ordovician icehouse. *Sci. Rep.* **6**, 18884 (2016).

112. M. R. Saltzman, S. A. Young, L. R. Kump, B. C. Gill, T. W. Lyons, B. Runnegar, Pulse of atmospheric oxygen during the late Cambrian. *Proc. Natl. Acad. Sci. U. S. A.* **108**, 3876–3881 (2011).

113. S. Scorrer, K. Azmy, S. Stouge, Carbon-isotope stratigraphy of the furongian berry head formation (Port au port group) and tremadocian watts bight formation (St. George Group), western newfoundland, and the correlative significance1. *Can. J. Earth Sci.* **56**, 223–234 (2019).

114. A. N. Sial, S. Peralta, C. Gaucher, A. J. Toselli, V. P. Ferreira, R. Frei, M. A. Parada, M. M. Pimentel, N. Silva Pereira, High-resolution stable isotope stratigraphy of the upper Cambrian and Ordovician in the Argentine Precordillera: Carbon isotope excursions and correlations. *Gondwana Res.* **24**, 330–348 (2013).

115. R. C. Wu, M. Calner, O. Lehnert, O. Peterffy, M. M. Joachimski, Lower-Middle Ordovician δ13C chemostratigraphy of western Baltica (Jämtland, Sweden). *Palaeoworld* **24**, 110–122 (2015).

116. R. Wu, M. Calner, O. Lehnert, Integrated conodont biostratigraphy and carbon isotope chemostratigraphy in the Lower-Middle Ordovician of southern Sweden reveals a complete record of the MDICE. *Geol. Mag.* **154**, 334–353 (2017).

117. S. A. Young, M. R. Saltzman, S. M. Bergström, Upper Ordovician (Mohawkian) carbon isotope (δ13C) stratigraphy in eastern and central North America: Regional expression of a perturbation of the global carbon cycle. *Palaeogeogr. Palaeoclimatol. Palaeoecol.* **222**, 53–76 (2005).

118. L. Zhang, T. J. Algeo, L. Cao, L. Zhao, Z. Q. Chen, Z. Li, Diagenetic uptake of rare earth elements by conodont apatite. *Palaeogeogr. Palaeoclimatol. Palaeoecol.* **458**, 176–197 (2016).

119. M. R. Saltzman, Silurian δ13C stratigraphy: a view from North America. *Geology* **29**, 671–674 (2001).

120. N. E. McAdams, M. D. Schmitz, M. A. Kleffner, J. Verniers, T. R. Vandenbroucke, J. R. Ebert, B. D. Cramer, A new, high-precision CA-ID-TIMS date for the 'Kalkberg' K-bentonite (Judds Falls Bentonite). *Lethaia* **51**, 344–356 (2018).

121. M. J. Melchin, C. Holmden, Carbon isotope chemostratigraphy of the Llandovery in Arctic Canada: Implications for global correlation and sea-level change. *GFF* **128**, 173–180 (2006).

122. J. C. Gouldey, M. R. Saltzman, S. A. Young, D. Kaljo, Strontium and carbon isotope stratigraphy of the Llandovery (Early Silurian): Implications for tectonics and weathering. *Palaeogeogr. Palaeoclimatol. Palaeoecol.* **296**, 264–275 (2010).

123. D. Kaljo, V. Grytsenko, T. Martma, M. A. Mõtus, Three global carbon isotope shifts in the Silurian of Podolia (Ukraine): Stratigraphical implications. *Est. J. Earth Sci.* **56**, 205–220 (2007).

124. B. D. Cramer, D. K. Loydell, C. Samtleben, A. Munnecke, D. Kaljo, P. Männik, T. Martma, L. Jeppsson, M. A. Kleffner, J. E. Barrick, C. A. Johnson, P. Emsbo, M. M. Joachimski, T. Bickert, M. R. Saltzman, Testing the limits of Paleozoic chronostratigraphic correlation via high-resolution (<500 k.y.) integrated conodont, graptolite, and carbon isotope (δ13Ccarb) biochemostratigraphy across the llandovery-Wenlock (Silurian) boundary: Is a unified Phanerozoic. *Bull. Geol. Soc. Am.* **122**, 1700–1716 (2010).

125. A. V. Hess, J. M. Trop, Sedimentology and carbon isotope (d13C) stratigraphy of Silurian-Devonian boundary interval strata, Appalachian Basin (Pennsylvania, USA). *Palaios* **34**, 405–423 (2019).

126. B. D. Cramer, M. A. Kleffner, M. R. Saltzman, The Late Wenlock Mulde positive carbon isotope (δ13Ccarb) excursion in North America. *GFF* **128**, 85–90 (2006).

127. M. R. Saltzman, Carbon isotope (δ13C) stratigraphy across the Silurian-Devonian transition in North America: Evidence for a perturbation of the global carbon cycle. *Palaeogeogr. Palaeoclimatol. Palaeoecol.* **187**, 83–100 (2002).

128. N. E. Buenger McAdams, Integrated carbon isotope chemostratigraphy and conodont biostratigraphy of the midcontinent Silurian, and a new date for the Devonian 'Kalkberg' K-bentonite, Ph.D. thesis, University of Iowa (2016).

129. S. C. Oborny, B. D. Cramer, C. E. Brett, A. M. Bancroft, Integrated Silurian conodont and carbonate carbon isotope stratigraphy of the east-central Appalachian Basin. *Palaeogeogr. Palaeoclimatol. Palaeoecol.* **554** (2020).

130. C. B. Waid, B. D. Cramer, Global chronostratigraphic correlation of the llandovery series (silurian system) in iowa, usa, using high-resolution carbon isotope (δ 13 c carb) chemostratigraphy and brachiopod and conodont biostratigraphy. *Bulletin of Geosciences* **92** (2017).

131. B. D. Cramer, M. R. Saltzman, Sequestration of 12C in the deep ocean during the early Wenlock (Silurian) positive carbon isotope excursion. *Palaeogeogr. Palaeoclimatol. Palaeoecol.* **219**, 333–349 (2005).

132. W. Buggisch, U. Mann, Carbon isotope stratigraphy of lochkovian to eifelian limestones from the devonian of central and southern europe. *International Journal of Earth Sciences* **93**, 521–541 (2004).

133. D. Chen, H. Qing, R. Li, The Late Devonian Frasnian-Famennian (F/F) biotic crisis: Insights from δ13Ccarb, δ13 Corg and 87Sr/86Sr isotopic systematics. *Earth Planet. Sci. Lett.* **235**, 151–166 (2005).

134. L. Ferrová, J. Frýda, P. Lukeš, High-resolution tentaculite biostratigraphy and facies development across the Early Devonian Daleje Event in the Barrandian (Bohemia): Implications for global Emsian stratigraphy. *Bull. Geosci.* **87** (2012).

135. K. Hillbun, T. E. Playton, E. Tohver, K. Ratcliffe, K. Trinajstic, B. Roelofs, S. Caulfield-Kerney, D. Wray, P. Haines, R. Hocking, D. Katz, P. Montgomery, P. Ward, Upper Kellwasser carbon isotope excursion pre-dates the F-F boundary in the Upper Devonian Lennard Shelf carbonate system, Canning Basin, Western Australia. *Palaeogeogr. Palaeoclimatol. Palaeoecol.* **438**, 180–190 (2015).

136. J. Hladíková, J. Hladil, B. Kříbek, Carbon and oxygen isotope record across Pridoli to Givetian stage boundaries in the Barrandian basin (Czech Republic). *Palaeogeogr. Palaeoclimatol. Palaeoecol.* **132**, 225–241 (1997).

137. J. M. Husson, B. Schoene, S. Bluher, A. C. Maloof, Chemostratigraphic and U-Pb geochronologic constraints on carbon cycling across the Silurian-Devonian boundary. *Earth Planet. Sci. Lett.* **436**, 108–120 (2016).

138. O. P. Izokh, N. G. Izokh, V. A. Ponomarchuk, D. V. Semenova, Carbon and oxygen isotopes in the Frasnian-Famennian section of the Kuznetsk basin (southern West Siberia). *Russ. Geol. Geophys.* **50**, 610–617 (2009).

139. A. A. Makhnach, B. G. Pokrovsky, O. V. Murashko, O. L. Petrov, Carbon and Oxygen Isotopes and Formation Conditions of the Upper Famennian Shale-Bearing Rocks in the Pripyat Trough, Southern Belarus. *Lithol. Miner. Resour.* **55**, 24–35 (2020).

140. K. Małkowski, G. Racki, A global biogeochemical perturbation across the Silurian-Devonian boundary: Ocean-continent-biosphere feedbacks (2009).

141. J. R. Morrow, C. A. Sandberg, K. Malkowski, M. M. Joachimski, Carbon isotope chemostratigraphy and precise dating of middle Frasnian (lower Upper Devonian) Alamo Breccia, Nevada, USA. *Palaeogeogr. Palaeoclimatol. Palaeoecol.* **282**, 105–118 (2009).

142. A. C. da Silva, F. Boulvain, Carbon isotope lateral variability in a Middle Frasnian carbonate platform (Belgium): Significance of facies, diagenesis and sea-level history. *Palaeogeogr. Palaeoclimatol. Palaeoecol.* **269**, 189–204 (2008).

143. P. J. Van Hengstum, D. R. Gröcke, Stable isotope record of the Eifelian-Givetian boundary Kačák-otomari Event (Middle Devonian) from Hungry Hollow, Ontario, Canada. *Can. J. Earth Sci.* **45**, 353–366 (2008).

144. J. J. Zambito, C. E. Brett, G. C. Baird, The late middle devonian (Givetian) Global Taghanic biocrisis in its type area (Northern Appalachian Basin): Geologically rapid faunal transitions driven by global and local environmental changes. *Earth Life Glob. Biodiversity, Extinction Intervals Biogeogr. Perturbations Through Time* (Springer Netherlands, 2012), pp. 677–703.

145. D. Zhang, Z. Tang, H. Huang, G. Zhou, C. Cui, Y. Weng, W. Liu, S. Kim, S. Lee, M. Perez-Neut, J. Ding, D. Czyz, R. Hu, Z. Ye, M. He, Y. G. Zheng, H. A. Shuman, L. Dai, B. Ren, R. G. Roeder, L. Becker, Y. Zhao, Metabolic regulation of gene expression by histone lactylation. *Nature* **574**, 575–580 (2019).

146. S. R. Cole, J. T. Haynes, P. C. Lucas, R. A. Lambert, Faunal and sedimentological analysis of a latest Silurian stromatoporoid biostrome from the central Appalachian Basin. *Facies* **61** (2015).

147. J. Liu, T. J. Algeo, W. Qie, M. R. Saltzman, Intensified oceanic circulation during Early Carboniferous cooling events: Evidence from carbon and nitrogen isotopes. *Palaeogeogr. Palaeoclimatol. Palaeoecol.* **531**, 108962 (2019).

148. D. Maharjan, G. Jiang, Y. Peng, R. A. Henry, Paired carbonate-organic carbon and nitrogen isotope variations in Lower Mississippian strata of the southern Great Basin, western United States. *Palaeogeogr. Palaeoclimatol. Palaeoecol.* **490**, 462–472 (2018).

149. L. S. Batt, I. P. Montañez, P. Isaacson, M. C. Pope, S. H. Butts, J. Abplanalp, Multi-carbonate component reconstruction of mid-carboniferous (Chesterian) seawater δ13C. *Palaeogeogr. Palaeoclimatol. Palaeoecol.* **256**, 298–318 (2007).

150. U. Brand, G. Jiang, K. Azmy, J. Bishop, I. P. Montañez, Diagenetic evaluation of a Pennsylvanian carbonate succession (Bird Spring Formation, Arrow Canyon, Nevada, U.S.A.) - 1: Brachiopod and whole rock comparison. *Chem. Geol.* **308-309**, 26–39 (2012).

151. W. Buggisch, X. Wang, A. S. Alekseev, M. M. Joachimski, Carboniferous–permian carbon isotope stratigraphy of successions from china (yangtze platform), usa (kansas) and russia (moscow basin and urals). *Palaeogeography, Palaeoclimatology, Palaeoecology* **301**, 18–38 (2011).

152. J. T. Koch, T. D. Frank, T. P. Bulling, Stable-isotope chemostratigraphy as a tool to correlate complex Mississippian marine carbonate facies of the Anadarko shelf Oklahoma and Kansas. *Am. Assoc. Pet. Geol. Bull.* **98**, 1071–1090 (2014).

153. A. G. Liu, C. G. Kenchington, E. G. Mitchell, Remarkable insights into the paleoecology of the Avalonian Ediacaran macrobiota (2015).

154. C. Liu, E. Jarochowska, Y. Du, D. Vachard, A. Munnecke, Stratigraphical and δ13c records of permo-carboniferous platform carbonates, south china: responses to late paleozoic icehouse climate and icehouse–greenhouse transition. *Palaeogeography, Palaeoclimatology, Palaeoecology* **474**, 113–129 (2017).

155. K. M. Meyer, M. Yu, D. Lehrmann, B. van de Schootbrugge, J. L. Payne, Constraints on Early Triassic carbon cycle dynamics from paired organic and inorganic carbon isotope records. *Earth Planet. Sci. Lett.* **361**, 429–435 (2013).

156. T. Galfetti, H. Bucher, A. Brayard, P. A. Hochuli, H. Weissert, K. Guodun, V. Atudorei, J. Guex, Late Early Triassic climate change: Insights from carbonate carbon isotopes, sedimentary evolution and ammonoid paleobiogeography. *Palaeogeogr. Palaeoclimatol. Palaeoecol.* **243**, 394–411 (2007).

157. G. Luo, T. J. Algeo, J. Huang, W. Zhou, Y. Wang, H. Yang, S. Richoz, S. Xie, Vertical δ 13 C org gradients record changes in planktonic microbial community composition during the end-Permian mass extinction. *Palaeogeogr. Palaeoclimatol. Palaeoecol.* **396**, 119–131 (2014).

158. A. Baud, V. Atudorei, Z. Sharp, Late permian and early triassic evolution of the northern indian margin: carbon isotope and sequence stratigraphy. *Geodin. Acta* **9**, 57–77 (1996).

159. K. E. Tierney, *Carbon and strontium isotope stratigraphy of the Permian from Nevada and China: Implications from an icehouse to greenhouse transition* (The Ohio State University, 2010).

160. W. Buggisch, K. Krainer, M. Schaffhauser, M. Joachimski, C. Korte, Late carboniferous to late permian carbon isotope stratigraphy: A new record from post-variscan carbonates from the southern alps (austria and italy). *Palaeogeography, Palaeoclimatology, Palaeoecology* **433**, 174–190 (2015).

161. C. Cheng, S. Li, X. Xie, T. Cao, W. L. Manger, A. B. Busbey, Permian carbon isotope and clay mineral records from the xikou section, zhen'an, shaanxi province, central china: climatological implications for the easternmost paleo-tethys. *Palaeogeography, Palaeoclimatology, Palaeoecology* **514**, 407–422 (2019).

162. K. T. Cramer, M. Bostic, High-resolution carbon isotope (δ13ccarb) chemostratigraphy of the lower permian from the us midcontinent: Checking the pulse of the late paleozoic ice age. *Bulletin* **127**, 584–595 (2015).

163. J. C. Laya, M. E. Tucker, D. R. Gröcke, A. Perez-Huerta, Carbon, oxygen and strontium isotopic composition of low-latitude permian carbonates (venezuelan andes): climate proxies of tropical pangea. *Geological Society, London, Special Publications* **376**, 367–385 (2013).

164. S.-z. Shen, C.-q. Cao, H. Zhang, S. A. Bowring, C. M. Henderson, J. L. Payne, V. I. Davydov, B. Chen, D.-x. Yuan, Y.-c. Zhang, *et al.*, High-resolution δ13ccarb chemostratigraphy from latest guadalupian through earliest triassic in south china and iran. *Earth and Planetary Science Letters* **375**, 156–165 (2013).

165. v. d. S. B. F. J. M. C. A. C. G. Bachan, Aviv, J. L. Payne, Carbon cycle dynamics following the end-Triassic mass extinction: Constraints from paired δ^{13}C$_c arb$ and δ^{13}C$_o rg$ records. *Geochemistry, Geophysics, Geosystems* **13** (2012).

166. C. Korte, S. P. Hesselbo, H. C. Jenkyns, R. E. Rickaby, C. Spötl, Palaeoenvironmental significance of carbon- and oxygen-isotope stratigraphy of marine Triassic-Jurassic boundary sections in SW Britain. *J. Geol. Soc. London.* **166**, 431–445 (2009).

167. R. Morante, A. Hallam, Organic carbon isotopic record across the Triassic-Jurassic boundary in Austria and its bearing on the cause of the mass extinction. *Geology* **24**, 391–394 (1996).

168. M. Hermoso, F. Minoletti, R. E. Rickaby, S. P. Hesselbo, F. Baudin, H. C. Jenkyns, Dynamics of a stepped carbon-isotope excursion: Ultra high-resolution study of Early Toarcian environmental change. *Earth Planet. Sci. Lett.* **319-320**, 45–54 (2012).

169. S. P. Hesselbo, H. C. Jenkyns, L. V. Duarte, L. C. Oliveira, Carbon-isotope record of the Early Jurassic (Toarcian) Oceanic Anoxic Event from fossil wood and marine carbonate (Lusitanian Basin, Portugal). *Earth Planet. Sci. Lett.* **253**, 455–470 (2007).

170. N. Preto, C. Agnini, M. Rigo, M. Sprovieri, H. Westphal, The calcareous nannofossil prinsiosphaera achieved rock-forming abundances in the latest triassic of western tethys: consequences for the δ 13 c of bulk carbonate. *Biogeosciences* **10**, 6053–6068 (2013).

171. W. Xu, M. Ruhl, H. C. Jenkyns, M. J. Leng, J. M. Huggett, D. Minisini, C. V. Ullmann, J. B. Riding, J. W. Weijers, M. S. Storm, *et al.*, Evolution of the toarcian (early jurassic) carbon-cycle and global climatic controls on local sedimentary processes (cardigan bay basin, uk). *Earth and Planetary Science Letters* **484**, 396–411 (2018).

172. R. Aguado, L. O'Dogherty, J. Sandoval, Calcareous nannofossil assemblage turnover in response to the early bajocian (middle jurassic) palaeoenvironmental changes in the subbetic basin. *Palaeogeography, Palaeoclimatology, Palaeoecology* **472**, 128–145 (2017).

173. J. Grabowski, V. Bakhmutov, Š. Kdỳr, M. Krobicki, P. Pruner, D. Reháková, P. Schnabl, K. Stoykova, H. Wierzbowski, Integrated stratigraphy and palaeoenvironmental interpretation of the upper kimmeridgian to lower berriasian pelagic sequences of the velykyi kamianets section (pieniny klippen belt, ukraine). *Palaeogeography, Palaeoclimatology, Palaeoecology* **532**, 109216 (2019).

174. G. Muttoni, M. Mazza, D. Mosher, M. E. Katz, D. V. Kent, M. Balini, A middle–late triassic (ladinian–rhaetian) carbon and oxygen isotope record from the tethyan ocean. *Palaeogeography, Palaeoclimatology, Palaeoecology* **399**, 246–259 (2014).

175. L. O'Dogherty, R. Aguado, P. O. Baumgartner, M. Bill, Š. Goričan, J. Sandoval, L. Sequeiros, Carbon-isotope stratigraphy and pelagic biofacies of the middle–upper jurassic transition in the tethys–central atlantic connection. *Palaeogeography, Palaeoclimatology, Palaeoecology* **507**, 129–144 (2018).

176. M. S. Storm, S. P. Hesselbo, H. C. Jenkyns, M. Ruhl, C. V. Ullmann, W. Xu, M. J. Leng, J. B. Riding, O. Gorbanenko, Orbital pacing and secular evolution of the early jurassic carbon cycle. *Proceedings of the National Academy of Sciences* **117**, 3974–3982 (2020).

177. X. Sun, T. Zhang, Y. Sun, K. L. Milliken, D. Sun, Geochemical evidence of organic matter source input and depositional environments in the lower and upper Eagle Ford Formation, south Texas. *Org. Geochem.* **98**, 66–81 (2016).

178. M. L. Gomes, M. T. Hurtgen, B. B. Sageman, Biogeochemical sulfur cycling during Cretaceous oceanic anoxic events: A comparison of OAE1a and OAE2. *Paleoceanography* **31**, 233–251 (2016).

179. J. S. Eldrett, C. Ma, S. C. Bergman, B. Lutz, F. J. Gregory, P. Dodsworth, M. Phipps, P. Hardas, D. Minisini, A. Ozkan, J. Ramezani, S. A. Bowring, S. L. Kamo, K. Ferguson,

C. Macaulay, A. E. Kelly, An astronomically calibrated stratigraphy of the Cenomanian, Turonian and earliest Coniacian from the Cretaceous Western Interior Seaway, USA: Implications for global chronostratigraphy. *Cretac. Res.* **56**, 316–344 (2015).

180. I. Jarvis, J. Trabucho-Alexandre, D. R. Gröcke, D. Uličný, J. Laurin, Intercontinental correlation of organic carbon and carbonate stable isotope records: evidence of climate and sea-level change during the Turonian (Cretaceous). *Depos. Rec.* **1**, 53–90 (2015).

181. J. O. Herrle, C. J. Schröder-Adams, W. Davis, A. T. Pugh, J. M. Galloway, J. Fath, Mid-cretaceous high arctic stratigraphy, climate, and oceanic anoxic events. *Geology* **43**, 403–406 (2015).

182. J. A. Moreno-Bedmar, J. Sandoval, J. Tavera, T. Bover-Arnal, R. Salas, G. Delanoy, F.-M. Maurrasse, R. Martínez, *et al.*, Lower aptian ammonite and carbon isotope stratigraphy in the eastern prebetic domain (betic cordillera, southeastern spain). *Geologica Acta* **10**, 333–354 (2012).

183. A. M. Oehlert, P. K. Swart, ARTICLE Interpreting carbonate and organic carbon isotope covariance in the sedimentary record. *Nat. Commun.* **5** (2014).

184. B. J. Tipple, M. Pagani, S. Krishnan, S. S. Dirghangi, S. Galeotti, C. Agnini, L. Giusberti, D. Rio, Coupled high-resolution marine and terrestrial records of carbon and hydrologic cycles variations during the Paleocene-Eocene Thermal Maximum (PETM). *Earth Planet. Sci. Lett.* **311**, 82–92 (2011).

185. E. M. Crouch, G. R. Dickens, H. Brinkhuis, M. P. Aubry, C. J. Hollis, K. M. Rogers, H. Visscher, The Apectodinium acme and terrestrial discharge during the Paleocene-Eocene thermal maximum: New palynological, geochemical and calcareous nannoplank-

ton observations at Tawanui, New Zealand. *Palaeogeogr. Palaeoclimatol. Palaeoecol.* **194**, 387–403 (2003).

186. A. Montanari, K. Farley, P. Claeys, D. De Vleeschouwer, N. De Winter, S. Vansteenberge, M. Sinnesael, C. Koeberl, Stratigraphic record of the asteroidal veritas breakup in the tortonian monte dei corvi section (ancona, italy). *Bulletin* **129**, 1357–1376 (2017).

187. A. D. Rooney, J. V. Strauss, A. D. Brandon, F. A. Macdonald, A Cryogenian chronology: Two long-lasting synchronous neoproterozoic glaciations. *Geology* **43**, 459–462 (2015).

188. K. J. Dennis, H. P. Affek, B. H. Passey, D. P. Schrag, J. M. Eiler, Defining an absolute reference frame for "clumped" isotope studies of CO2. *Geochim. Cosmochim. Acta* **75**, 7117–7131 (2011).

189. S. M. Bernasconi, M. Daeron, K. D. Bergmann, M. Bonifacie, A. N. Meckler, C. InterCarb, A community effort to improve interlaboratory standardization of the carbonate clumped isotope thermometer. *Geochemistry, Geophys. Geosystems* p. https://doi.org/10.1002/essoar.10504430.2.

190. N. T. Anderson, C. A. Cowan, K. D. Bergmann, A case for the growth of ancient ooids within the sediment pile. *J. Sediment. Res.* **90**, 843–854 (2020).

191. J. Horita, Oxygen and carbon isotope fractionation in the system dolomite–water–CO2 to elevated temperatures. *Geochim. Cosmochim. Acta* **129**, 111–124 (2014).

192. A. Matthews, A. Katz, Oxygen isotope fractionation during the dolomitization of calcium carbonate. *Geochim. Cosmochim. Acta* **41**, 1431–1438 (1977).

193. C. Vasconcelos, J. A. McKenzie, R. Warthmann, Calibration of the δ18O paleothermometer for dolomite precipitated in microbial cultures and natural environments. *Geology* (2005).

194. B. H. Passey, N. E. Levin, T. E. Cerling, F. H. Brown, J. M. Eiler, K. K. Turekian, High-temperature environments of human evolution in East Africa based on bond ordering in paleosol carbonates. *Proc. Natl. Acad. Sci. U. S. A.* **107**, 11245–11249 (2010).

195. K. W. Huntington, J. M. Eiler, H. P. Affek, W. Guo, M. Bonifacie, L. Y. Yeung, N. Thiagarajan, B. Passey, A. Tripati, M. Daëron, R. Came, Methods and limitations of 'clumped' CO 2isotope (Δ 47) analysis by gas-source isotope ratio mass spectrometry. *J. Mass Spectrom.* **44**, 1318–1329 (2009).

196. S. Bernasconi, Reducing uncertainties in carbonate clumped isotope analysis through consistent carbonate-based standardization. *Geochem. Geophys. Geosyst.* **19**, 2895–2914 (2018).

197. A. J. Schauer, J. Kelson, C. Saenger, K. W. Huntington, Choice of 17O correction affects clumped isotope (Δ 47) values of CO2 measured with mass spectrometry. *Rapid Commun. Mass Spectrom.* **30**, 2607–2616 (2016).

198. M. Daëron, D. Blamart, M. Peral, H. P. Affek, Absolute isotopic abundance ratios and the accuracy of D 47 measurements. *Chem. Geol.* **442**, 83–96 (2016).

199. D. B. CM John, Community software for challenging isotope analysis: First applications of 'Easotope' to clumped isotopes. *Rap. Commun. Mass Spec.* **30**, 2285–2300 (2016).

200. P. K. Swart, S. J. Burns, J. J. Leder, Fractionation of the stable isotopes of oxygen and carbon in carbon dioxide during the reaction of calcite with phosphoric acid as a function of temperature and technique. *Chem. Geol. Isot. Geosci. Sect.* **86**, 89–96 (1991).

201. J. Rosenbaum, S. M. F. Sheppard, An isotopic study of siderites, dolomites and ankerites at high temperatures. *Geochim. Cosmochim. Acta* **50**, 1147–1150 (1986).

202. M. Bonifacie, D. Calmels, J. M. Eiler, J. Horita, C. Chaduteau, C. Vasconcelos, P. Agrinier, A. Katz, B. H. Passey, J. M. Ferry, J. J. Bourrand, Calibration of the dolomite clumped isotope thermometer from 25 to 350 °C, and implications for a universal calibration for all (Ca, Mg, Fe)CO3 carbonates. *Geochim. Cosmochim. Acta* **200**, 255–279 (2017).

203. I. Müller, Clumped isotope fractionation during phosphoric acid digestion of carbonates at 70°C. *Chem. Geol.* **449**, 1–14 (2017).

204. E. Grosjean, G. D. Love, C. Stalvies, D. A. Fike, R. E. Summons, Origin of petroleum in the Neoproterozoic-Cambrian South Oman Salt Basin. *Org. Geochem.* **40**, 87–110 (2009).

205. G. D. Love, E. Grosjean, C. Stalvies, D. A. Fike, J. P. Grotzinger, A. S. Bradley, A. E. Kelly, M. Bhatia, W. Meredith, C. E. Snape, S. A. Bowring, D. J. Condon, R. E. Summons, Fossil steroids record the appearance of Demospongiae during the Cryogenian period. *Nature* **457**, 718–721 (2009).

206. M. K. Lloyd, U. Ryb, J. M. Eiler, Experimental calibration of clumped isotope reordering in dolomite. *Geochim. Cosmochim. Acta* **242**, 1–20 (2018).

207. M. K. Lloyd, J. M. Eiler, P. I. Nabelek, Clumped isotope thermometry of calcite and dolomite in a contact metamorphic environment. *Geochim. Cosmochim. Acta* **197**, 323–344 (2017).

208. S. L. Goldberg, T. M. Present, S. Finnegan, K. D. Bergmann, A highresolution record of early Paleozoic climate. *Proceedings of the National Academy of Sciences* **118** (2021).

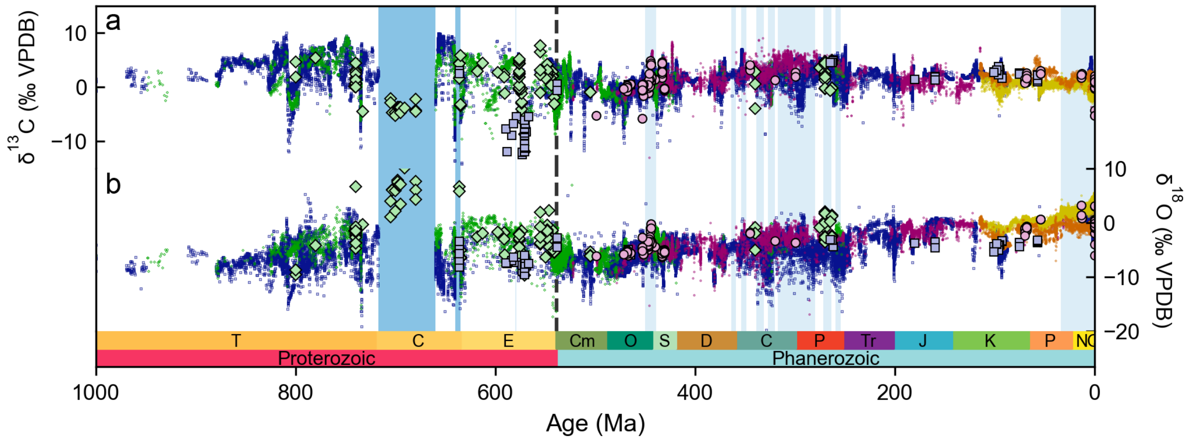

Fig. 1. Carbonate mineral δ^{13}C and δ^{18}O values through the last 1 Ga (**a**) δ^{13}C of limestone rocks (blue squares), dolomite rocks (green diamonds), shallow marine coastal fossils (purple circles), planktonic foraminifera (orange circles), benthic foraminifera (yellow circles), and Δ_{47} samples (lighter colors, same symbols). (**b**) δ^{18}O values with same symbology as above. Vertical bars indicate events: two Snowball Earth glaciations (dark blue), high latitude glaciations (light blue), and the Neoproterozoic–Phanerozoic boundary (dashed black line).

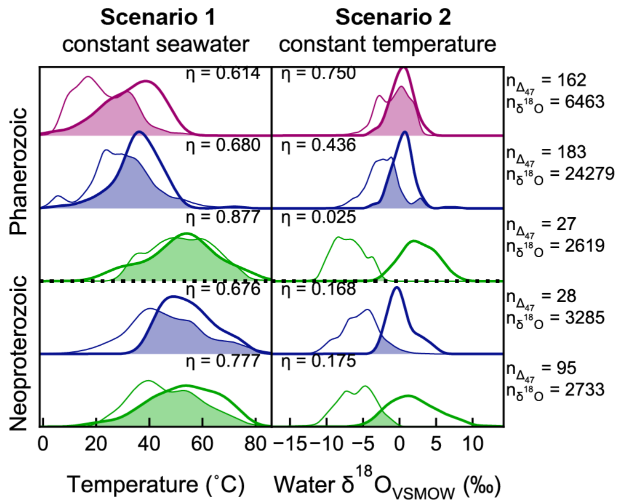

Fig. 2. A comparison of Scenario 1 vs. Δ_{47}-temperature and Scenario 2 vs. Δ_{47}-derived water δ^{18}O$_{VSMOW}$ (**a**) Phanerozoic fossil (purple), limestone rock (blue), and dolomite (green) and Neoproterozoic limestone (blue), and dolomite rock (green) Gaussian kernel density estimates (KDE) of δ^{18}O translated under the assumptions of Scenario 1 (thin line) compared to Phanerozoic fossil Δ_{47}-temperature (thick line). The overlap (η) between the two is shaded and number of overlap points is reported. The number of samples used in each KDE is to the right of the plot. Scenario 1 assumes mineral δ^{18}O depends only on temperature using a water δ^{18}O$_{VSMOW}$ value of -1.2‰ to calculate temperature (*23–25*). (**b**) Phanerozoic and Neoproterozoic Gaussian kernel density estimates of δ^{18}O translated under the assumptions of Scenario 2 (thin line) compared to Δ_{47}-derived water δ^{18}O$_{VSMOW}$ (thick line). Scenario 2 assumes the mineral δ^{18}O increase depends only on changing seawater δ^{18}O. Seawater temperature is held at a constant 25°C to calculate seawater δ^{18}O (*23–25*).

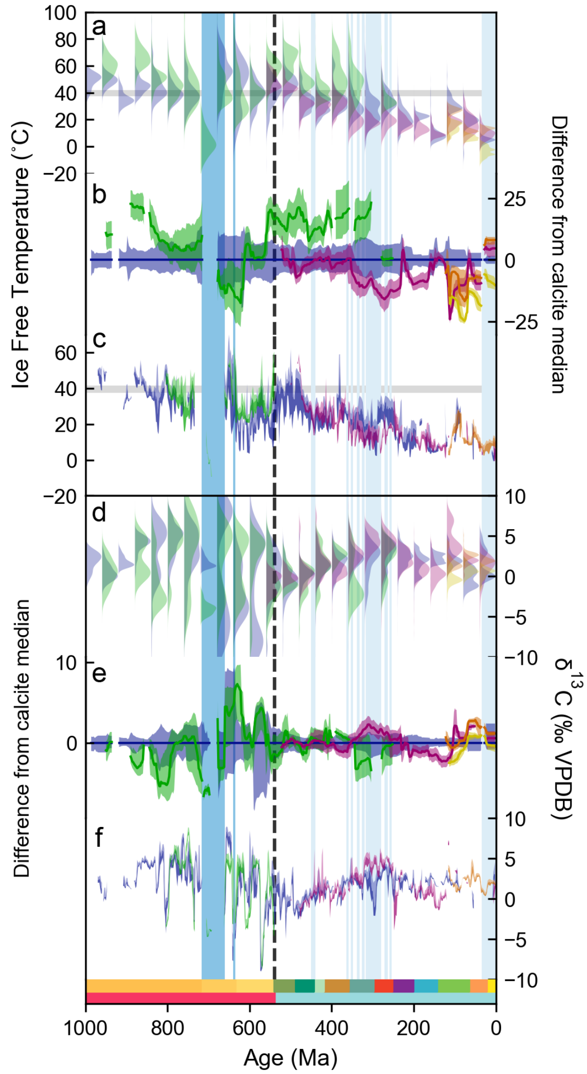

Fig. 3. Temperature and δ^{13}C temporal variability by material. (**a,d**) Distribution of temperature estimates from Scenario 1 and δ^{13}C in 40 Myr windows estimated using Gaussian kernel density estimates for limestone rocks (blue), dolomite rocks (green), shallow marine coastal fossils (purple), planktonic foraminifera (orange), and benthic foraminifera (yellow). (**b,e**) dolomite (green) and coastal fossil (purple) lines are the difference from of their respective medians from the calcite median (blue) for temperature (b) and δ^{13}C (c). The shaded envelopes are the 25th and 75th quantiles. The limestone median is zero and the colored envelop represents

the 25^{th} and 75^{th} quantiles using Gaussian kernel density estimates in 40 Myr window. (**c**) The included temperature data for Fig. 4 by material, the 1^{st} to 50^{th} quantiles of Scenario 1 temperature with a moving distribution with a 4 Myr window sampled each 2 Myr by type. No dolomite in the Phanerozoic and early Neoproterozoic (>800 Ma) is included. (**f**) The median of δ^{13}Cvalues, with a shaded envelop from the 25 to 75^{th} quantiles with a moving distribution sampling each 1 Ma with a window of 5 Myr by type. No dolomite in the Phanerozoic and early Neoproterozoic (>800 Ma) is included. Vertical bars indicate events: two Snowball Earth glaciations (dark blue), high latitude glaciations (light blue), and the Neoproterozoic–Phanerozoic boundary (dashed black line).

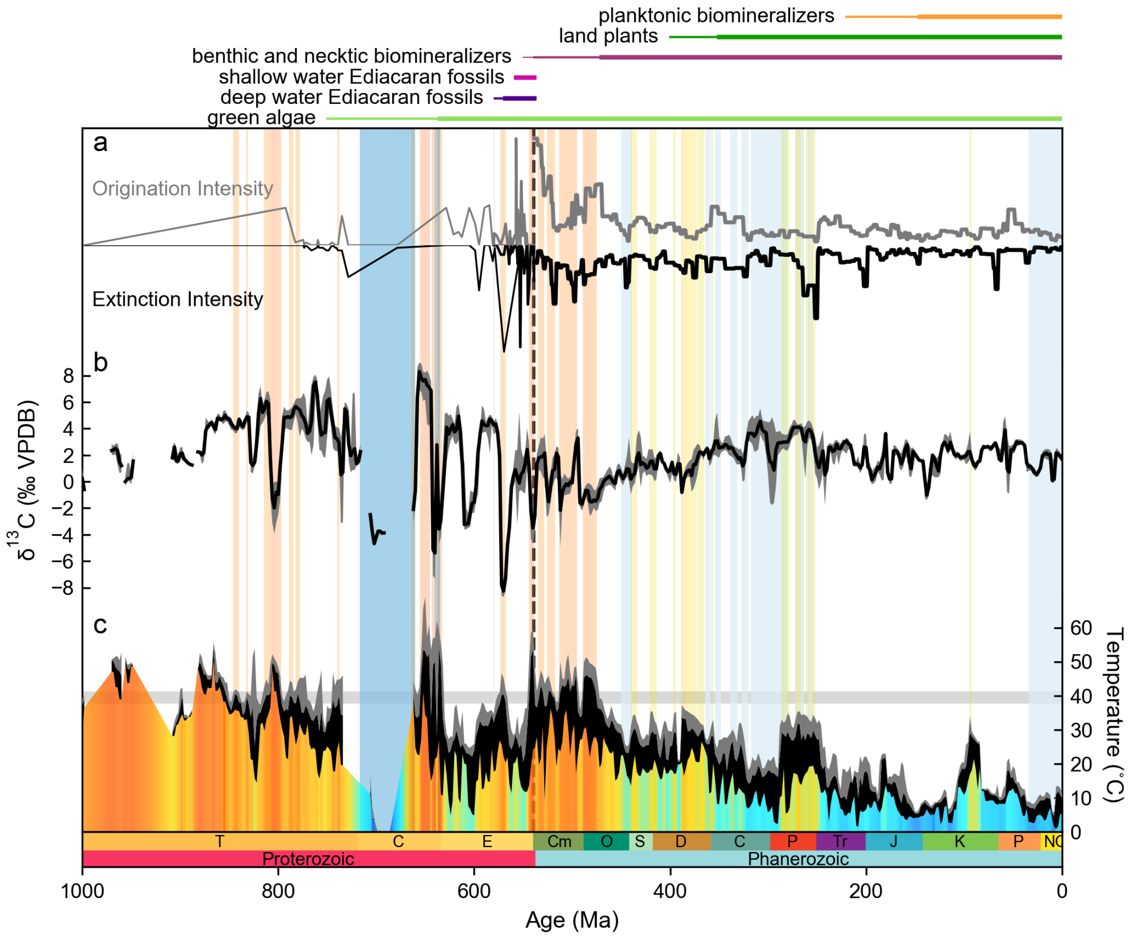

Fig. 4. Critical radiations in the history of life, δ^{13}C, and a tropical temperature record (**a**) Estimates of origination and extinction intensities following (*50*) for Neoproterozoic microfossils using data from (*51, 53, 56*)(thin line in Neoproterozoic), macroscopic Ediacaran fossils using data from (*54*)(medium line in Ediacaran), and fossil marine genera (*50*)(thick line in Phanerozoic). (**b**) Median of δ^{13}C values, with a 25-75$^{\text{th}}$ shaded envelop with a moving distribution sampling each 1 Ma with a window of 5 Myr from Fig. 3f. (**c**) The 5-50$^{\text{th}}$ quantiles of coastal, shallow marine, tropical temperatures from Scenario 1 with a moving distribution sampling each 1 Ma with a window of 5 Myr. Before 440 Ma, intervals $>$ 1 Myr with a 25$^{\text{th}}$ quantile temperature $>$ 38°C are extended to the top of the plot. After 440 Ma, intervals $>$ 1 Myr with

a 25th quantile temperature $> 28°C$ are extended. Grey band represents the upper temperature limit of modern tropical subtidal ectotherms (*62*). Vertical bars indicate events: two Snowball Earth glaciations (dark blue), high latitude glaciations (light blue), and the Neoproterozoic–Phanerozoic boundary (dashed black line).

Supplementary Materials for: A billion years of temperature variability: a key driver of Earth's long-term habitability

Authors:

Kristin D. Bergmann, Nicholas Boekelheide, Julia W. Clarke,
Marjorie D. Cantine, Julia Wilcots, Noah T. Anderson,
Adam B. Jost, Olivia Laub, Juliana Drozd, Samuel L. Goldberg,
Tyler Mackey, Fran Meyer, Athena Eyster

1 Materials and Methods

Mineral δ^{18}O compilation A literature search was conducted to locate published mineral δ^{18}O data from shallow platform carbonates spanning 1.5 Ga to the modern. Most of this data was associated with high-resolution δ^{13}C studies, usually sampled at meter-resolution. The δ^{18}O data from these datasets from bulk rocks had not been previously compiled. Isotopic datasets from the literature were then digitized into .csv files, and metadata were added (location, mineralogy, formation, etc.).

Data included in mineral δ^{18}O compilation :

Mesoproterozoic: (*22, 63–68*)

Neoproterozoic: (*13, 21, 22, 69–90*)

Cambrian: (*72, 91–99*)

Ordovician: (*91, 94, 96, 100–118*)

Silurian: (*119–131*)

Devonian: (*125, 127, 132–146*)

Carboniferous: (*147–154*)

Permo-Triassic: (*151, 154–164*)

Triassic-Jurassic: (*165–177*)

Cretaceous: (*178–182*)

Cenozoic: (*183–186*)

Fossils: (*5, 6, 15*) with only tropical/subtropical used

Clumped: (*11–13, 16, 17*)

Age Model We created a consistent age model for all individual studies and opted not to use previously published age models individual authors may have created. In the Phanerozoic, we used the Geologic Time Scale 2020 to set period, stage, and age boundaries (*19*). Regional stage boundaries were used where applicable. We also used the GTS2020 to add additional tie points based on biostratigraphy (i.e., trilobite, conodont, and graptolite zones) and δ^{13}C excursions. Age models were built using information provided within the datasets, stratigraphic columns, and text of compiled articles. At the upper and lower boundaries of datasets when no other tie point could be found, the midpoint between the nearest tie point within the section and the next reasonable age tie point was used as an estimated age tie point. For all points in the dataset, ages were interpolated using a linear model assuming a constant sedimentation rate between tie points. Sedimentation rates were error checked for consistency. The age model for compiled δ^{18}O Proterozoic datasets utilized U/Pb and Re/Os ages from the published literature (*20–22, 187*) and δ^{13}C excursions were used to build a new age model for each study.

Scenario 1 and 2 calculations We have gathered mineralogical information for all samples in the δ^{18}O compilation so that we can explore the implications of Scenario 1 and Scenario 2. This mineralogical information was collected from stratigraphic columns and data tables. We used mineral-specific fractionation factors to calculate either water δ^{18}O using T = 25°C (Scenario 1) or temperature using a water $\delta^{18}O_{VSMOW}$ value of -1.2‰(Scenario 2). Mineral-specific fractionation factors for calcite samples (*23*) and dolomite samples (*24*).

Δ_{47} compilation Carbonate Δ_{47} data was compiled from (*11–13,16,17*) and references therein. Results in (*16*) were screened to remove all Arctic and Antarctic carbonates and all Cretaceous Interior Seaway carbonates to provide the best constraints on marine, tropical carbonate platforms through time. Results from (*13*) are recalculated (see below), whereas all other measurements were not analyzed with sufficient ETH-1–4 carbonate standards to use the I-CDES. We estimate this may affect temperatures by $\sim$5°C or less and will not alter the results in Fig. 2.

Materials for new Δ_{47} analyses All new samples presented are dolomite and were provided by Andrew Knoll. Three samples are from the Kotuikan Formation in the Anbar Uplift, Siberia (KG_92_21, KG_92_24, KG_92_27B, plotted at 1450 Ma), Five samples are from the Dismal Lakes Group in N.W.T. (DL_2_B, DL_1_B, DL_1_A, DL_1_D, DL_2_A, plotted at 1300 Ma). Five samples are from the Svanbergfjellet Formation, Svalbard (G3_129f_A, G3129f_B,G3_135.6, G3_157.2_B, G3_157.2_A, plotted at 780 Ma). Four samples are from the Thule Group, NW Greenland (KS_78_12A, KS_78_12_B, KS_78_22, KS_78_7, plotted at 1150 Ma). Three samples are from the Wynniatt Formation and Reynolds Point Formation, Shaler Group (88_KL_119, 88_KL_68_A, 88_KL_100, 88_KL_68_B, 88_KL_108_B, 88_KL_108_A, plotted at 802 Ma and 830 Ma respectively). Three samples are from the Pendjari Supergroup, Volta Basin, Burkina Faso (PK99_KT_4c_A, PK99_KT_3A, PK99_KT4C_B, plotted at 635 Ma).

Methods for new Δ_{47} analyses A selection of the previously unpublished Precambrian samples described above were analyzed at the MIT Carbonate Research Lab on a Nu Perspective dual-inlet isotope ratio mass spectrometer coupled to a NuCarb automated sample preparation unit held at 70°C with 4 or more replicates. Approximately 450 μg of sample powder was drilled from polished sample slabs and digested in sample vials with 150 μL 104% phosphoric acid (H_3PO_4). Evolved CO_2 was purified cryogenically and by passage through a porapak trap (1/4" inner diameter tube filled with 0.4 g 50-80 mesh PorapakQ bracketed by silver wool) held at $-30°C$. After purification, evolved CO_2 was transferred to a cold finger in a microvolume and warmed to room temperature. Reference gas pressure was balanced to match the sample beam size. Beam intensities were collected in three blocks of 20 integration cycles of 20 seconds each. Voltage on the m/z 44 beam at the start of each analysis is 8–20 V; this is depleted by approximately 50% over replicate analysis.

The NuCarb autosampling device is equipped with a 50-vial carousel that is analyzed over $\sim$ 80 hours. Four carbonate standards (ETH-1, ETH-2, ETH-3, and ETH-4) were used to transfer Δ_{47} values to the Carbon Dioxide Equilibrium Scale (CDES) (*188*) using 25°C acid temperature anchor values from the InterCarb interlaboratory comparison project (*189*). Laboratory protocols for the distribution of standards throughout the 50-vial carousel changed over the course of this study. Prior to February 2018, queues were planned for $>$18 ETH standards alongside in-house standards and $<$23 unknown samples; after this point, 22 ETH standards were included in each run, along with three additional standards (IAEA-C1, IAEA-C2, and MERCK) and 25 unknowns. Uncommon shorter runs (i.e. $<$50 vials) exceeded the 1:1 sample:standard ratio. Analytical failures due to autosampler or gas transfer malfunction led to differences between planned standard:unknown distributions and actual analyses. Final Δ_{47} temperatures were calculated using the calibration equation of (*190*). As all samples are dolomite, Δ_{47}-derived water δ^{18}O were calculated using (*191–193*) and results using the equation from (*191*) are presented in Fig. 2.

We provide a reanalysis of temperatures from (*13*) using the standard values for ETH-1, ETH-2, ETH-3, and ETH-4 from the InterCarb interlaboratory comparison project (*189*) and final Δ_{47} temperatures using the calibration equation of (*190*). Δ_{47}-derived water $\delta^{18}O_{VSMOW}$ values were calculated using (*23, 191–193*) and dolomite samples using the equation from (*191*) are presented in Fig. 2.

All of the new Precambrian samples were also analyzed 1-2 times at Caltech in 2015. Methods follow those outlined in (*12*). Samples of 9–12 mg of powder were weighed into silver capsules before being reacted in a phosphoric common acid bath ($\sim 103\%; 1.90 \leq \rho \leq 1.92$) for 20 minutes at 90°C. Evolved CO_2 was collected and purified with an automated acid digestion and gas purification device as described by (*194*). This device includes passing the CO_2 through multiple cryogenic traps using either a dry ice and ethanol mix or liquid nitrogen as well as through a Porapak-Q 120/80 mesh gas chromatography column held at -20°C using a helium carrier gas. Sulfur was scrubbed from the CO_2 using an in-line silver wool trap. The CO_2 was measured on the ThermoFinnigan MAT 253 IRMS, nicknamed 'Admiral' housed at Caltech. Each measurement consisted of eight acquisitions (16V on m/z = 44) of seven cycles of unknown sample CO_2 versus Oztech working gas as outlined by (*195*). Best practices in the clumped-isotope community have evolved to better address pressure baseline issues, nonlinearity in the source, scale compression, and necessary sample replication (e.g., (*189, 196–198*). We input raw measurement files of 1000°C heated and 25°C equilibrated gases and carbonate standard data along with raw measurement files of sample unknowns into Easotope, an open-source software tool specifically developed for clumped isotope data processing (*199*). The carbonate δ^{18}O values were calculated using a 90°C acid-digestion fractionation factor for calcite from (*200*) and for dolomite (*201*). Carbonate δ^{13}C and δ^{18}O values were drift-corrected using a 10 standard moving window to a NBS-19 and NBS-19 calibrated internal Carrara Marble standard (CIT). We corrected all of the Δ_{47} data using a 10 standard moving window using heated gases, equilibrated gases, and two carbonate standards (CIT, TV04) for both the linearity correction and empirical transfer function into the carbon dioxide equilibrated scale (CDES) as defined by (*188*). To better represent the true uncertainty the error on each sample is presented as 2SE, twice the commonly reported 1SE (see (*202, 203*)). A Caltech-derived temperature calibration from (*202*)(Eq. 3) was used for CDES90. As all samples are dolomite, Δ_{47}-derived water δ^{18}O were calculated using (*191–193*) and results using the equation from (*191*) are presented in Fig. 1, S1, S2.

Figure Methods The distributions in Fig. 2 are generated on the unweighted points using Gaussian kernel density estimates as implemented in the scipy package in python with bandwidth selected using Scott's Rule. The overlap η is the fraction of the distributions that overlay each other. It is estimated as the area under the minimum of the distributions along the curves.

The distributions in Fig. 3a,d and the moving distributions in Fig. 3b,e are generated using Gaussian kernel density estimates as above with window of 40 Myr. Windows with fewer than 14 points are excluded. The moving distributions are sampled each 2 Myr. The moving quartiles in Fig. 3c,f are estimated using quantile regression on points within 4 Myr windows sampled each 2 Myr. The first quartile is approximated using the 1^{st} to 25^{th} quantile, and the fourth quartile is approximated using the 75^{th} to 99^{th}. Only the first and second quartiles are shown in Fig. 3c,f. All of the quartiles are shown as Scenario 1 and 2 in Fig. S1.

The origination and extinction intensities in the Neoproterozoic in Fig. 4a are estimated using lists of taxa identified through time. The origination intensity is the number of species that appear from one bin to the next. The extinction intensity is the number of species that disappear from one bin to the next. The Neoproterozoic Ediacaran fauna data are from (*54*), Neoproterozoic microfossils are from (*51–53*), the Phanerozoic extinction and origination intensities are from (*50*). Moving quartiles in Fig. 4b,c are generated as described above for Fig. 3. The δ^{13}C record is plotted using the 2^{nd} and 3^{rd} quartiles (25^{th} to 75^{th} quantiles). The temperature record is plotted using the 1^{st} and 2^{nd} quartiles (1^{st} to 50^{th} quantile).

2 Supplemental Materials

Solid-state reordering and elevated Δ_{47}-temperatures We are undoubtedly presenting Δ_{47}-temperatures that have experienced solid state reordering, particularly from Precambrian strata. Solid-state reordering would result in "apparent" enriched water δ^{18}O compositions. Thus, one could argue if all of our Precambrian samples have experienced significant solid state reordering, we have no basis for assessing seawater δ^{18}O through time. We think our data set merits consideration for the following reasons: [1] Δ_{47}-temperature results are from six different Precambrian carbonate platforms, some of which yield intact biomarkers (*204, 205*). It is unlikely that all of these locations experienced similar degrees of solid state reordering. [2] Multiple samples throughout the record approach or sit at or near water δ^{18}O composition of -1.2‰ including bulk rock samples from both the Phanerozoic and Precambrian indicating bulk rocks can lithify early, record seawater $\delta^{18}O_{VSMOW}$ values, and preserve them for hundreds of millions of years, [3] Almost all of the Precambrian samples are dolomite which has been shown to be more resistant to solid state reordering than calcite (*206, 207*). It is also relevant for considerations of the δ^{18}O 'bulk' rock compilation that our Δ_{47} results in multiple locations (both in the Phanerozoic and Precambrian (*11–13, 208*)), suggest that populations of carbonates in carbonate platforms often lithify in the presence of minimal fluids (i.e. the pore fluids become buffered by the carbonate rocks and new fluids are not introduced) which lends more plausibility to interpreting the Δ_{47}-derived water $\delta^{18}O_{VSMOW}$ results largely as a primary record. In summary, we have found the clumped isotope record is more easily altered by lithification and subsequent post-depositional alteration than mineral δ^{18}Obut not so much that it looses all meaning in many shallowly buried locations. Both records preserve stratigraphic trends that suggest long-term (and shorter term) climate change.

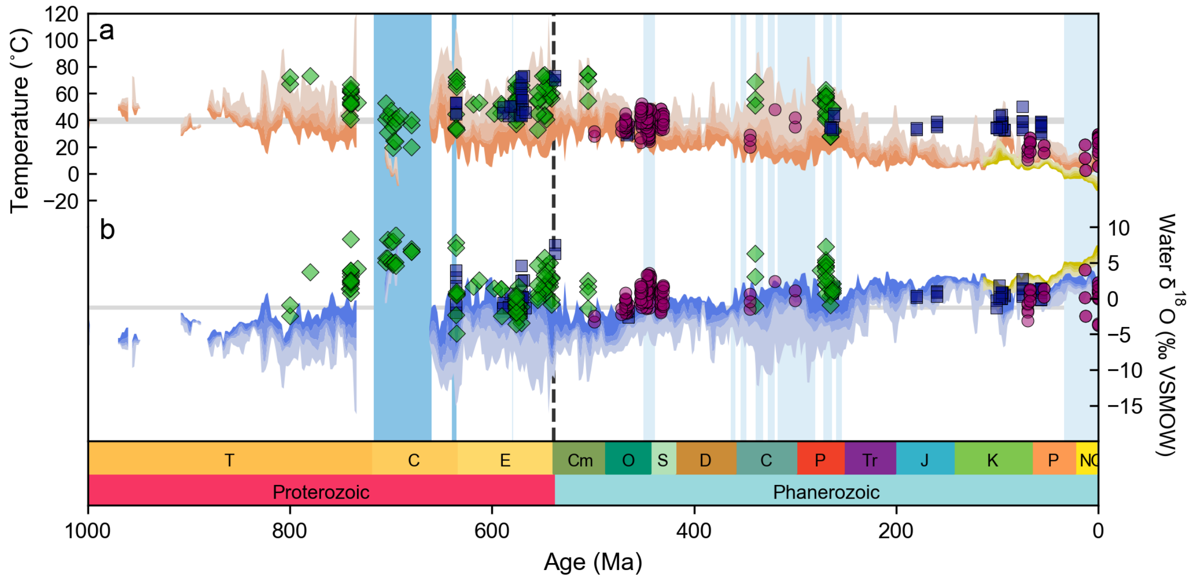

Fig. S1. Scenario 1 and Scenario 2 compared to Δ_{47}-temperature and Δ_{47}-derived water $\delta^{18}\mathrm{O}_{VSMOW}$ values (**a**) Scenario 1 assumes mineral δ^{18}O depends only on temperature. Seawater $\delta^{18}\mathrm{O}_{VSMOW}$ is held at a constant value of -1.2‰to calculate temperature (*23–25*). Δ_{47}-temperature values (larger symbols) are compared to Scenario 2. Results are plotted as quantiles of a moving distribution sampling each 1 Ma with a window of 5 Ma. (**b**) Scenario 2 assumes the mineral δ^{18}O increase depends only on changing seawater δ^{18}O. Seawater temperature is held at a constant 25°C to calculate seawater δ^{18}O (*23–25*). Horizontal line indicates -1.2‰ seawater expected from Cenozoic ice-free conditions (*26, 27*). Results are plotted as quantiles of a moving distribution sampling each 1 Ma with a window of 5 Ma. Δ_{47}-derived water $\delta^{18}\mathrm{O}_{VSMOW}$values (*23–25*) are compared to Scenario 2 (larger symbols). Vertical light blue boxes indicate periods of glaciation. Dolomite rocks (green diamonds), limestone rocks (blue squares), and calcite, aragonite and apatite fossils (purple circles).

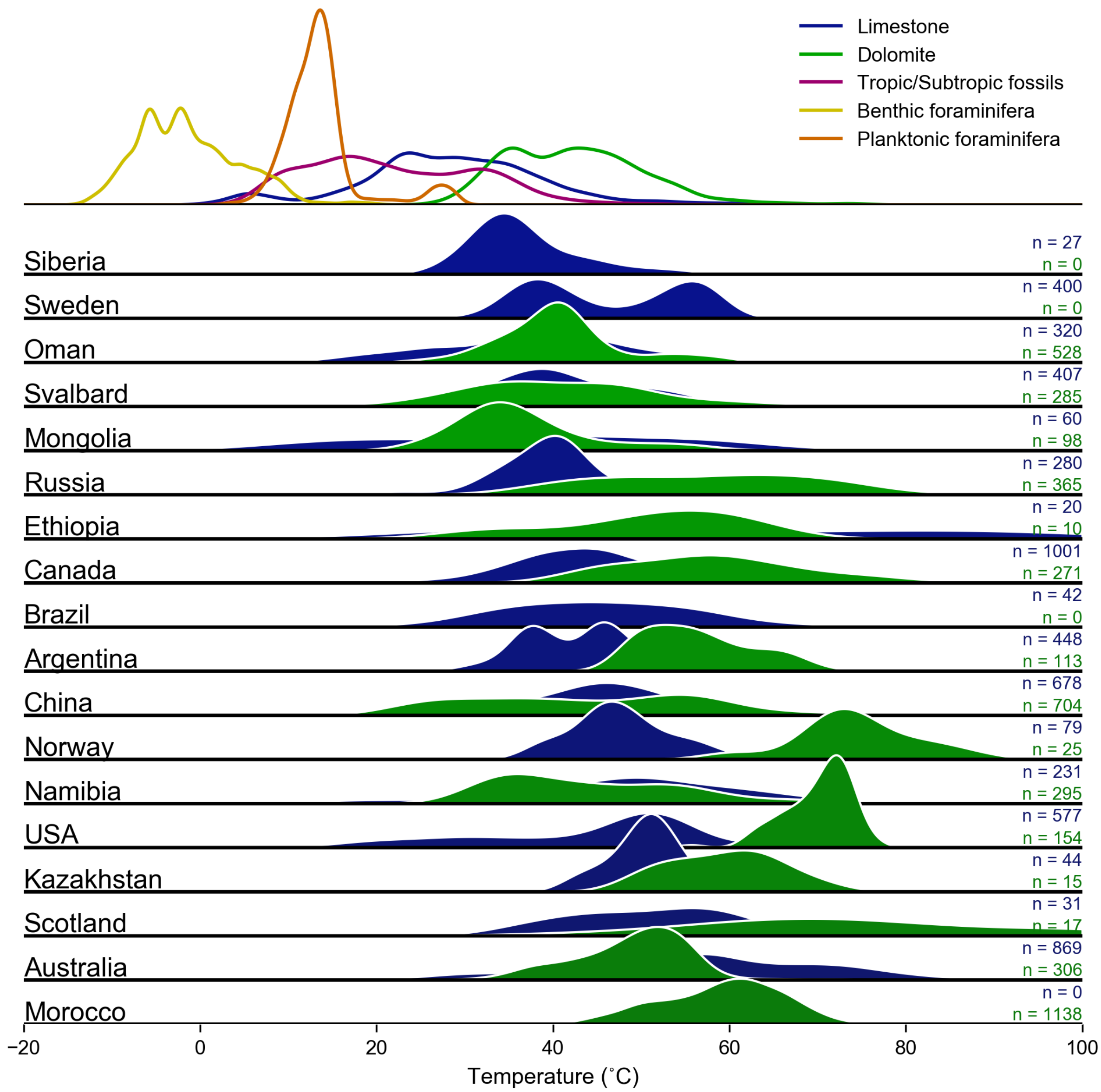

Fig. S2. Neoproterozic Scenario 1 temperatures by location for limestone (blue) and dolomite (green) rocks compared to the Phanerozoic distributions..

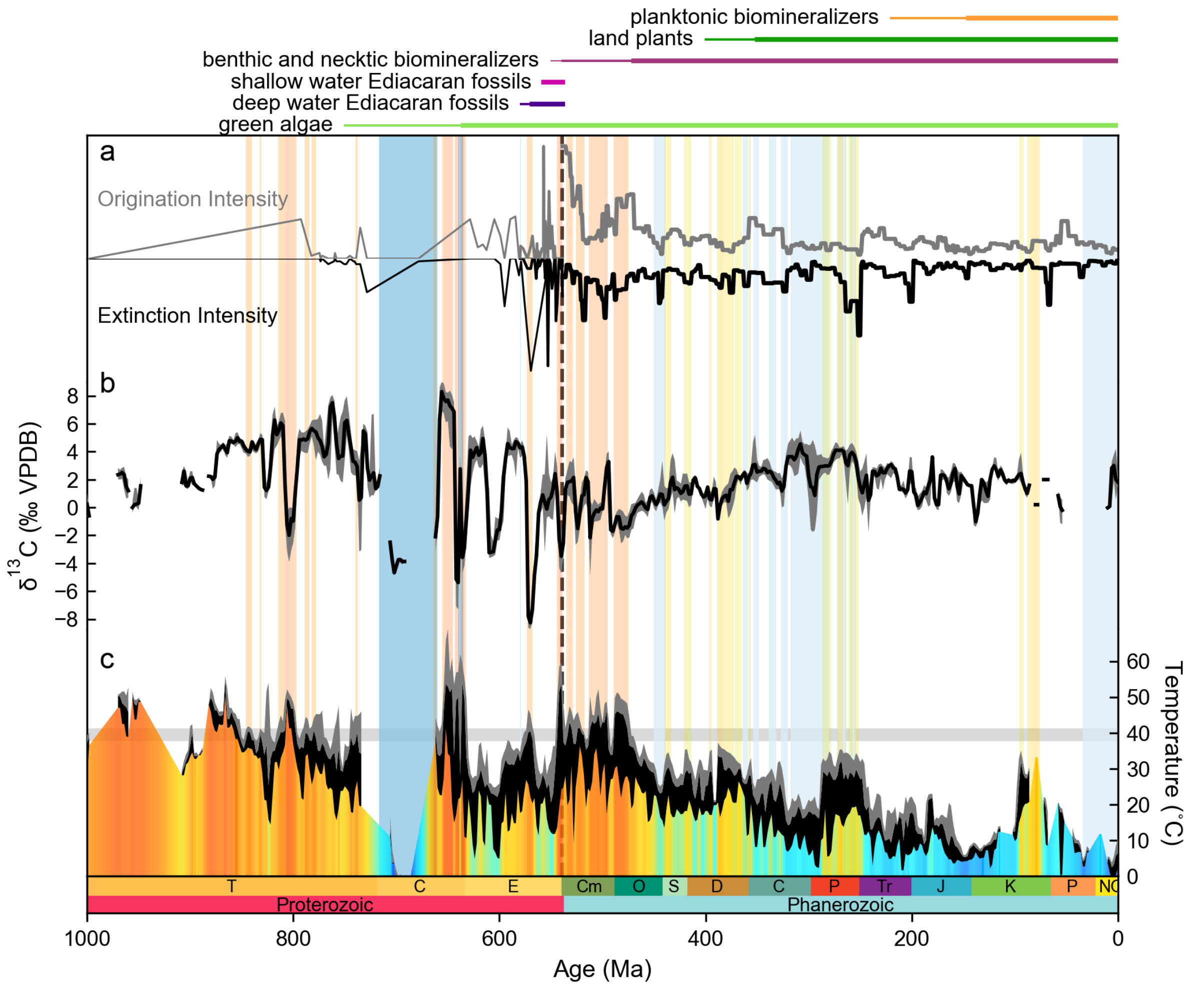

Fig. S3. Exploration of the effects of removing planktonic foraminfera from Fig. 4. (**a**) Estimates of origination and extinction intensities following (*50*) for Neoproterozoic microfossils using data from (*51, 53, 56*)(thin line in Neoproterozoic), macroscopic Ediacaran fossils using data from (*54*)(medium line in Ediacaran), and fossil marine genera (*50*)(thick line in Phanerozoic). (**b**) Median of δ^{13}C values, with a 25-75$^{\text{th}}$ shaded envelop with a moving distribution sampling each 1 Ma with a window of 5 Myr from Fig. 3f. (**c**) The 5-50$^{\text{th}}$ quantiles of coastal, shallow marine, tropical temperatures from Scenario 1 with a moving distribution sampling each 1 Ma with a window of 5 Myr. Before 440 Ma, intervals $>$ 1 Myr with a 25$^{\text{th}}$ quantile temperature $>$ 38°C are extended to the top of the plot. After 440 Ma, intervals $>$ 1 Myr with a 25$^{\text{th}}$ quantile temperature $> 28°$C are extended. Grey band represents the upper temperature limit of modern tropical subtidal ectotherms (*62*). Vertical bars indicate events: two Snowball Earth glaciations (dark blue), high latitude glaciations (light blue), and the Neoproterozoic–Phanerozoic boundary (dashed black line). Cenozoic temperatures are not significantly warmer than in Fig. 4. which may reflect shift in carbonate precipitation to mid-latitudes.